ELEMENTA
Science of the Anthropocene

Primary production calculations for sea ice from bio-optical observations in the Baltic Sea

Susann Müller[1,2*] • Anssi V. Vähätalo[1,3] • Jari Uusikivi[1,4] • Markus Majaneva[1,2,4] • Sanna Majaneva[1,4] • Riitta Autio[4] • Janne-Markus Rintala[1,2]

[1]University of Helsinki, Helsinki, Finland
[2]Tvärminne Zoological Station, Hanko, Finland
[3]University of Jyväskylä, Department of Biological and Environmental Science, Jyväskylä, Finland
[4]Finnish Environment Institute (SYKE), Marine Research Centre, Helsinki, Finland
*susann.mueller@helsinki.fi

Abstract

Bio-optics is a powerful approach for estimating photosynthesis rates, but has seldom been applied to sea ice, where measuring photosynthesis is a challenge. We measured absorption coefficients of chromophoric dissolved organic matter (CDOM), algae, and non-algal particles along with solar radiation, albedo and transmittance at four sea-ice stations in the Gulf of Finland, Baltic Sea. This unique compilation of optical and biological data for Baltic Sea ice was used to build a radiative transfer model describing the light field and the light absorption by algae in 1-cm increments. The maximum quantum yields and photoadaptation of photosynthesis were determined from ^{14}C-incorporation in photosynthetic-irradiance experiments using melted ice. The quantum yields were applied to the radiative transfer model estimating the rate of photosynthesis based on incident solar irradiance measured at 1-min intervals. The calculated depth-integrated mean primary production was 5 mg C m^{-2} d^{-1} for the surface layer (0–20 cm ice depth) at Station 3 (fast ice) and 0.5 mg C m^{-2} d^{-1} for the bottom layer (20–57 cm ice depth). Additional calculations were performed for typical sea ice in the area in March using all ice types and a typical light spectrum, resulting in depth-integrated mean primary production rates of 34 and 5.6 mg C m^{-2} d^{-1} in surface ice and bottom ice, respectively. These calculated rates were compared to rates determined from ^{14}C incorporation experiments with melted ice incubated *in situ*. The rate of the calculated photosynthesis and the rates measured *in situ* at Station 3 were lower than those calculated by the bio-optical algorithm for typical conditions in March in the Gulf of Finland by the bio-optical algorithm. Nevertheless, our study shows the applicability of bio-optics for estimating the photosynthesis of sea-ice algae.

Domain Editor-in-Chief
Jody W. Deming, University of Washington

Associate Editor
Jean-Éric Tremblay, Université Laval

Knowledge Domain
Ocean Science

Article Type
Research Article

Part of an *Elementa* Special Feature
Biogeochemical Exchange Processes at Sea-Ice Interfaces (BEPSII)

Received: May 29, 2015
Accepted: June 29, 2016
Published: September 1, 2016

Introduction

Optical properties and bio-optical modelling of primary production are well described in sea water (e.g., Morel, 1988; Behrenfeld and Falkowski, 1997), compared to sea ice (Perovich, 2003; Ehn et al., 2004; Zhao et al., 2010; Ehn and Mundy, 2013; Nicolaus and Katlein, 2013). For example, spectral absorption by phytoplankton has frequently been separated from non-algal particles in seawater (Kishino et al., 1985) but seldom in sea ice (Piiparinen et al., 2015). Sympagic organisms inhabiting the surface layers of sea ice are also exposed to solar ultraviolet radiation (UVR) without the possibility of mixing with deeper layers as in seawater, making them particularly vulnerable to UVR damage (Gibson et al., 2000; Piiparinen, 2011). The optical properties of sea ice at the spectral range of UVR have been reported only in a few studies (Ehn et al., 2004; Uusikivi et al., 2010).

Estimating primary production in seawater is directly based on photosynthetic carbon fixation (reviewed in Falkowski and Raven, 2007). Applying methods developed for seawater to sea-ice research is challenging due to the structural differentiation of sea ice into ice and brine, and the high variability concerning its

physical and biogeochemical properties. Nevertheless, the commonly used ^{14}C technique has also been applied to sea-ice samples that were melted and incubated in vitro (Piiparinen et al., 2010; Enberg et al., 2015). Another study treated sea-ice slices with ^{14}C bicarbonate and incubated them in their original position in the ice sheet (Mock and Gradinger, 1999). Other attempts to estimate primary production in undisturbed sea ice have used diving pulse-amplitude-modulated (PAM) fluorometers (Rysgaard et al., 2001) or oxygen optodes and microelectrodes (McMinn and Ashworth, 1998; Rysgaard et al., 2001; Glud et al., 2002; Mock et al., 2003). Underwater eddy covariance has recently also been tested to estimate net primary production based on a combination of velocity and oxygen measurements (Long et al., 2012). All methods have significant constraints and the "true" primary production in sea ice therefore remains unknown.

The varying types and histories of ice (Stoecker et al., 2000) result in a variety of sea ice properties with a high level of patchiness. Sampling conditions are concurrently difficult and constrain primary production measurements. Earlier publications reporting measured primary production rates only present data for one or a few time points per day, usually representing high light conditions (Lizotte and Sullivan, 1992; Rysgaard et al., 2001). Only Stoecker et al. (2000) measured the primary production in sea ice *in situ* for 24 h. But realistic means per day and month are necessary to gain a daily or seasonal estimate of the photosynthesis rate depending on the physico-biogeochemical conditions in the ice. Model development is hence important for the large-scale and long-term estimation of optical properties and the calculation of light-dependent primary production.

Primary production has long been estimated based on photosynthesis-irradiance (PI) data, where the maximum photosynthetic rate (P_m), chlorophyll *a* (Chl *a*) and the saturation parameter of photosynthesis (E_k) are used to calculate a photosynthesis rate (Jassby and Platt, 1976; Platt et al., 1980; Smith et al., 1989; Arrigo and Sullivan, 1994, Ehn and Mundy, 2013); see Appendix for abbreviations. Another approach is based on the absorption by phytoplankton, quantum yield of photosynthesis and downwelling irradiance (Kiefer and Mitchell, 1983; Morel, 1991). Certain models use fluorescence measurements to validate the model or satellite data to obtain basic data (Subramaniam et al, 1999; Raateoja et al., 2004; Tedesco et al., 2010). Algal pigment data and under-ice irradiances have recently been used to calculate algal biomass (Melbourne-Thomas et al., 2015). To our knowledge, a model calculating primary production based on measured PI relationships for Baltic Sea ice or for the entire ice column does not exist. The very limited number of data sets addressing optical properties combined with primary production in Baltic Sea ice makes the development and validation of models challenging.

Models calculating optical properties of sea ice based on optical measurements have been published by Arrigo (1997), Ehn et al. (2008b), Uusikivi et al. (2010) and Ehn and Mundy (2013), but only the models by Arrigo (Arrigo, 1997; Arrigo and Sullivan, 1994) and Ehn and Mundy (2013) have been used to also calculate primary production rates. Furthermore, complex ecosystem models exist for calculating primary production based on physical and biogeochemical fluxes in the ocean, atmosphere and sea ice (Tedesco et al., 2012; Vancoppenolle et al., 2013).

Here we present a data set for Baltic Sea ice that includes optical measurements, such as incoming and transmitted irradiance and albedo, and spectral (from 300 nm to 700 nm) absorption coefficients of CDOM (a_{CDOM}), algae (a_{algae}) and de-pigmented particles (a_d) in sea ice, and measurements of photosynthetic efficiency and 24-h *in situ* primary production rates using melted sea ice. These data were collected for three different ice types at different locations in the Gulf of Finland (GoF) together with a fourth station during the following year. They were used to develop an algorithm to compute the primary production for GoF sea ice in March, based on a data set that represents the typical bio-optical conditions in GoF sea ice in mid-March. The combination of optical measurements with photosynthetic efficiency and primary production measurements enabled us to calculate a quantum yield for photosynthesis in sea ice and estimate primary production rates at a 1-cm vertical resolution.

Materials and methods

Sampling

Sea ice was examined at four stations in the Gulf of Finland (GoF), Baltic Sea (Table 1). Samples were collected during a cruise of R/V *Aranda* in March 2010 in the GoF, which was entirely ice-covered at the time, at three stations (hereafter called St.1, St.2, and St.3), and on fast ice near Tvärminne on the southern coast of Finland in February 2011 at one station (hereafter called St.4). The sampling sites represented the following different ice types (Table 1): drift ice (St.1), deformed fast ice (St.2) and level fast ice (St.3 and St.4). (The ice at St.2 is hereafter called deformed ice, and the ice at St.3 and St.4 is hereafter called fast ice.) The drift ice at St.1 was covered by 8–10 cm of snow and 1–2 cm of refrozen snow, and the deformed ice at St.2 was covered by 5–6 cm snow. The fast ice at St.3 had probably been flooded, resulting in a 6-cm layer of snow over a 7-cm slush layer (slush meaning mixed snow and seawater) on top of the ice, the lowest 1 cm of which was very icy. The slush was sampled using a clean polyethylene (PE) container and then treated and analysed in the same way as the ice samples. The structural analysis of thin sections (Weeks and

Table 1. Sampling stations, environmental conditions and physical parameters for 4–5 layers of sea ice and under-ice water

Station, ice type	Ice depth [cm; n = 3 to 5]	Location, date	Weather, ice cover	Temperature [°C]	Salinity	Ice layer[a]
St.1, drift ice	0–11	59° 55.7' N 26° 01.1' E, 9 March 2010	Sunny, –3.6 °C, 7.5 cm snow	–1.8	1.5	surface
	11–22			–1.25	1.1	surface
	22–32			–0.9	1.1	bottom
	32–42			–0.75	0.9	bottom
	42–51.5			–0.7	0.8	bottom
	UIW			3.8	5.2	-
	mean surface: 0–22	-	-	**–1.4**	**1.3**	-
	mean bottom: 22–51.5	-	-	**–0.8**	**0.9**	-
St.2, deformed fast ice	0–15	60° 14.3' N 26° 37.6' E, 11 March 2010	Cloudy, 0.3 °C, 5.3 cm snow	–0.98	0.8	surface
	15–30			–1.0	0.9	surface
	30–47			–0.8	0.7	bottom
	47–65			–0.55	0.8	bottom
	65–82.5			–0.5	0.7	bottom
	mean surface: 0–30	-	-	**–1.0**	**0.9**	-
	mean bottom: 30–82.5	-	-	**–0.6**	**0.7**	-
St.3,[a] level fast ice	0–11	60° 19.7' N 26° 51.7' E, 13 March 2010	Sunny, air –2.6 °C, 6 cm snow, 7 cm slush	–0.5	0.9	surface
	11–22			–0.6	0.6	surface
	22–33			–0.7	0.4	bottom
	33–44			–0.7	0.5	bottom
	44–55			–0.65	0.4	bottom
	UIW			3.7	3.4	-
	mean surface: 0–22	-	-	**–0.6**	**0.8**	-
	mean bottom: 22–55	-	-	**–0.7**	**0.4**	-
St.4,[b] level fast ice	0–5	59° 51' N 23° 16' E, 28 February 2011	Sunny, air –8 °C, 6.0 cm snow	-	0.8	surface
	5–10			-	0.4	surface
	10–26			-	0.8	surface
	26–36			-	0.9	bottom
	mean surface: 0–26	-	-	-	**0.7**	-
	mean bottom: 26–36	-	-	-	**0.9**	-

[a]At St.3, the ice layers were assigned to surface and bottom based on granular and columnar ice crystals, respectively, observed in a thin section of ice core. At St.4, the surface and bottom layers were defined based on the high a_d in surface layers due to atmospheric deposition close to the coast. For other stations, the ice between 0 and 22 cm was assigned as surface layer.
[b]Data for St.4 were obtained from Enberg et al. (2015).
doi: 10.12952/journal.elementa.000121.t001

Gow, 1978) showed that the upper 20 cm at St.3 consisted of snow-ice formed partly from re-frozen slush and transitional ice, and the lower 36 cm consisted of columnar ice. At each station, seven replicate cores were taken using a motorised ice-coring system (9-cm internal diameter, Kovacs Enterprises). One core was used to determine the vertical temperature distribution of the ice at 5-cm intervals using a Testo 915-1 thermometer (at all stations) and one (at St.1 and St. 3) was analysed for ice texture. The remaining cores were sectioned within 1 min after sampling into five layers of approximately equal thickness and pooled into a PE bag (Mercamer Oy) for biological and biogeochemical analyses. The mean thicknesses of the ice cores and their vertical layers are reported in Table 1, but the thicknesses of individual cores varied between 43 and 66 cm at St.1, between 50 and 112 cm at St.2 and between 55 and 57 cm at St.3. The replicates of each layer were pooled and transported in darkness at air temperature to R/V *Aranda* where they were crushed and melted overnight. The melting samples were kept cool (≤ 4 °C) and in darkness overnight as explained in Rintala et al. (2014). The melted samples were split as soon as possible for further analysis. Salinity was measured from the melted samples using a YSI 63 meter. Melted samples were filtered through GF/F for pigment analysis and absorption measurements.

At St.4, three replicate cores were collected and cut into four pieces (Table 1). The three replicate cores of each vertical layer were pooled for optical measurements (CDOM and POM) and chlorophyll *a* concentrations.

Under-ice water (UIW) was sampled at St.1–3 through the corer hole after removal of slush using a 1-litre PE bottle washed with ultrapure water (Milli-Q). UIW at St.4 was sampled using a Limnos water sampler. The UIW was stored at 4 °C and its absorption properties were analysed together with the melted ice samples.

Irradiance measurements

The incident, reflected and transmitted spectral irradiances were measured simultaneously with three Ramses-ACC VIS spectroradiometers (TriOS GmbH) at St.3. These measurements were carried out on undisturbed ice cover, originally with snow cover on top, after removing approximately 2 m^2 of the snow cover with a shovel.

These spectroradiometers measured upwelling or downwelling plane irradiances from 320 nm to 950 nm at 3.3-nm intervals using a cosine collector. Measurements from two of the sensors were normalised to match the measurements from the third sensor from a cross-calibration of all sensors in air. To measure transmitted irradiances, an aluminium arm with floats was used to position one sensor under the ice. The arm was installed through a 30 x 30 cm hole in the ice and the sensor was positioned 3 cm below the ice bottom, 1 m south of the hole. Irradiance measurements were expressed as an average of at least three successive measurements.

Photosynthetically active radiation (PAR, 400–700 nm) was measured at St.3 with the Ramses instruments between 11:00 and 14:00 local time two to ten times every hour. PAR outside of these measurements was calculated from continuous measurements (at 1-min intervals) of incident integrated shortwave radiation (SW) (Middleton, Carter-Scott Manufacturing Pty. Ltd. Melbourne, Australia EP-16 pyranometer, spectral range 300–3000 nm) assuming a constant ratio between PAR and SW during the *in situ* measurements in cloud-free weather. This PAR to SW ratio was obtained from simultaneous spectral irradiance (using Ramses instruments) and SW measurements.

Chlorophyll a measurements

Chlorophyll *a* (Chl *a*) concentrations were measured by fluorometry from particles of melted ice retained by GF/F filters, which were stored frozen at –20 °C until analysis. Chl *a* extraction was performed using 96% v/v EtOH during 24 h at room temperature in the dark. After re-filtering the extract through Whatman GF/F filters the fluorescence was measured with a Jasco FP-750 spectrofluorometer. The calculation of Chl *a* concentrations was performed according to HELCOM (1988).

Absorption coefficients

The absorption coefficient of particles retained by the GF/F filters were measured within a few hours from the sample collection (UIW) or after melting (sea ice) with a Shimadzu UV-VIS 2550 spectrophotometer using an integrating sphere (ISR-240 A) and the "transmittance-reflectance" method by Tassan and Ferrari (2002). The transmittance and reflectance of the GF/F-filters on a quartz support were measured from 200 nm to 750 nm at 1-nm intervals with a 2-nm slit width. The absorption coefficient of all particles, $a_t(\lambda)$, was calculated from their optical densities accounting for the path length amplification and the ratio of filtered volume to filter area (Tassan and Ferrari, 2002). The coloured particles on the filters were bleached with sodium hypochlorite and re-measured for the absorption coefficient of de-pigmented particles, $a_d(\lambda)$ (Ferrari and Tassan, 1999). The absorption coefficient of photo-autotrophs, $a_{algae}(\lambda)$, was calculated as the difference between $a_t(\lambda)$ and $a_d(\lambda)$. The mean absorption of a_{algae} at 747 to 750 nm was subtracted from the absorption at each wavelength $a_{algae}(\lambda)$ (Babin et al., 2003). For a Chl *a*-specific absorption coefficient, $a_{algae}(\lambda)^*$, values for $a_{algae}(\lambda)$ were divided by the concentration of chlorophyll *a* determined from the aliquot.

The absorption coefficient of CDOM, $a_{CDOM}(\lambda)$, was determined from the GF/F filtrates of melted ice. The absorbance by CDOM, $A_{CDOM}(\lambda)$, was measured against Milli-Q water from 200 nm to 700 nm at 1-nm intervals with a 2-nm slit width on Shimadzu UV-VIS spectrophotometers using a 10-cm quartz cuvette. The absorption coefficient of CDOM, $a_{CDOM}(\lambda)$, was calculated as:

$$a_{CDOM}(\lambda) = 2.303 A_{CDOM}(\lambda) l^{-1} \quad (1)$$

where 2.303 transforms 10-based logarithm to e-based logarithm and l is the path length of the cuvette in metres (0.1).

The spectral slopes of CDOM, $S_{250–450}$, $S_{275–295}$ and $S_{350–400}$, and of de-pigmented particles, $S_{380–730}$, were calculated by nonlinear fitting in MATLAB from

$$a_\lambda = a_{\lambda_0} e^{S(\lambda_0 - \lambda)} \quad (2)$$

where λ_0 describes the shortest wavelength of the spectral range for $S_{\lambda 0–\lambda}$ (Stedmon et al., 2000). The slope ratio, SR, was calculated for CDOM as $S_{275–295}/S_{350–400}$ (Helms et al., 2008).

The total absorption coefficient for the ice layers, $a_t(\lambda)$, was calculated as:

$$a_t(\lambda) = a_{i+b}(\lambda) + a_{CDOM}(\lambda) + a_d(\lambda) + a_{algae}(\lambda) \quad (3)$$

where $a_{i+b}(\lambda)$ is the volume-weighted average absorption coefficient of 95% pure ice (Grenfell and Perovich, 1981; Perovich and Govoni, 1991) and 5% clear ocean water as brine (Smith and Baker, 1981; Sogandares and Fry, 1997). The selected brine volume (5%) was based on earlier measurements in the same area by Ehn et al. (2004). For the snow layer, partly flooded with seawater (St.3) and partly frozen, $a_t(\lambda)$ was calculated according to:

$$a_t(\lambda) = a_i(\lambda)(\rho_{snow}/\rho_{ice})d_{ice}d_{total}^{-1} + ((a_{CDOM,slush}(\lambda) + a_{d,slush}(\lambda) + a_{algae,slush}(\lambda))d_{slush}d_{total}^{-1} \quad (4)$$

The first part of the equation describes absorption by pure snow defined as a product of $a_i(\lambda)$, the absorption of pure ice (Grenfell and Perovich, 1981), and ρ_{snow}/ρ_{ice}, the ratio of snow density at the sampling station (ρ_{snow} = 0.26 g cm^{-3}) to the density of ice (ρ_{ice} = 0.92 g cm^{-3}). The latter part describes the measured absorption properties of slush. The layer thickness of snow and slush, respectively, is described by the parameter d relative to the total layer thickness. If no slush has formed on top of the ice (St.1, St.2, St.4), then absorption will only be calculated from the absorption of pure snow and the density ratio that accounts for the partly re-frozen snow.

The total absorption of snow for mean fast ice and GoF ice was calculated using a more general approach, as the absorption properties of the flooded layer are not always known. The absorption properties of snow were combined with absorption properties of UIW, where the ratio of flooded snow (including UIW) to the total thickness of the total snow layer was defined by d_{frozen} to d_{total} using

$$a_t(\lambda) = a_i(\lambda)(\rho_{snow}/\rho_{ice}) + (a_{CDOM,UIW}(\lambda) + a_{d,UIW}(\lambda) + a_{algae,UIW}(\lambda)d_{frozen}d_{total}^{-1}) \quad (5)$$

Primary production measurements

The primary production of sympagic communities was determined as ^{14}C incorporation incubations based on Steeman-Nielsen (1952) and modified after Rintala et al. (2014). Two different approaches were used: 24-h *in situ* incubations to estimate the daily net primary production at St.1 and St.3, and 2–3 h laboratory incubations for photosynthesis-irradiance (PI) responses to use the values for maximum photosynthetic rate, P_m, and maximum light utilisation coefficient, α, from each sample for primary production calculations in the algorithm.

The *in situ* incubations were performed using pooled melted sea ice from each of the five vertical layers. Each of five 20-ml subsamples of each pooled sample, introduced into glass scintillation vials, received 50 µl $NaH^{14}CO_3$ (final concentration of 0.05 µCi ml^{-1}). Two of the five vials of each layer were wrapped in aluminium foil to block all penetration of light and be used as dark controls. For the *in situ* incubation, a 10-cm deep hole was drilled in the ice next to the sampling site. The scintillation vials were placed in the hole at ambient light at a 10-cm depth for 24 h, covered with the ice core of the same hole and a layer of snow representing the depth of snow cover on ice. The chosen depth represented the mean light level of the surface layer (Table 1). The sample taken from the uppermost ice layer was incubated at a deeper layer and hence, lower light level, while the three samples from the deepest layers were exposed to higher light levels than at their sampling depth.

The PI incubations were performed using 18 subsamples (with 3-ml sample volume) of melted sea ice that was pipetted into 7-ml glass scintillation vials with added $NaH^{14}CO_3$ (50 µl, final concentration of 0.33 µCi ml^{-1}; International Agency for ^{14}C, DHI). The vials were incubated at 4 °C for 2–3 h in the PI response incubators using two replicates at each light intensity (E_d) between 0 and 1500 µmol PAR m^{-2} s^{-1} including two dark controls. The lamps used had an emission maximum at 659 nm. The incubators were cooled by circulating ice-cold water with a peristaltic pump.

Both of the incubations were stopped with 100 µl of formaldehyde (final concentration 1.23%) and acidified with 1 N HCl to remove the unincorporated $NaH^{14}CO_3$. Insta-Gel Plus (PerkinElmer) scintillation cocktail was added to the acidified samples and the activity was measured with a Wallac WinSpectral 1414 liquid scintillation counter. For sea-ice samples, total inorganic carbon was calculated from the linear correlation between salinity and TIC based on Kuosa (unpublished).

The primary production rate (P; µg C m^{-3} h^{-1}) and the primary production rate normalized to Chl *a* (P^*; µg C µg Chl a^{-1} h^{-1}) versus the downwelling incident PAR (E_d; µmol photons m^{-2} s^{-1}) from PI incubations (Figure 1) were fitted using the Curve Fitting toolbox in MATLAB (Mathworks Inc., MA, USA) to:

$$P^* = P_m(1 - \exp[(-\alpha E_d)P_m^{-1}]\exp[(-\beta E_d)P_m^{-1}] \quad (6)$$

where P_m is the maximum photosynthetic rate (µg C m^{-3} h^{-1} or µg C µg Chl a^{-1} h^{-1}), α is the maximum light utilisation coefficient (mg C mg Chl a^{-1} [m^2 µmol photons]$^{-1}$) and β is the photoinhibition parameter (Platt et al., 1980; Setälä, 2004). Negative replicates of the P values were not included in the calculations as they indicate an incomplete mixing of the sample.

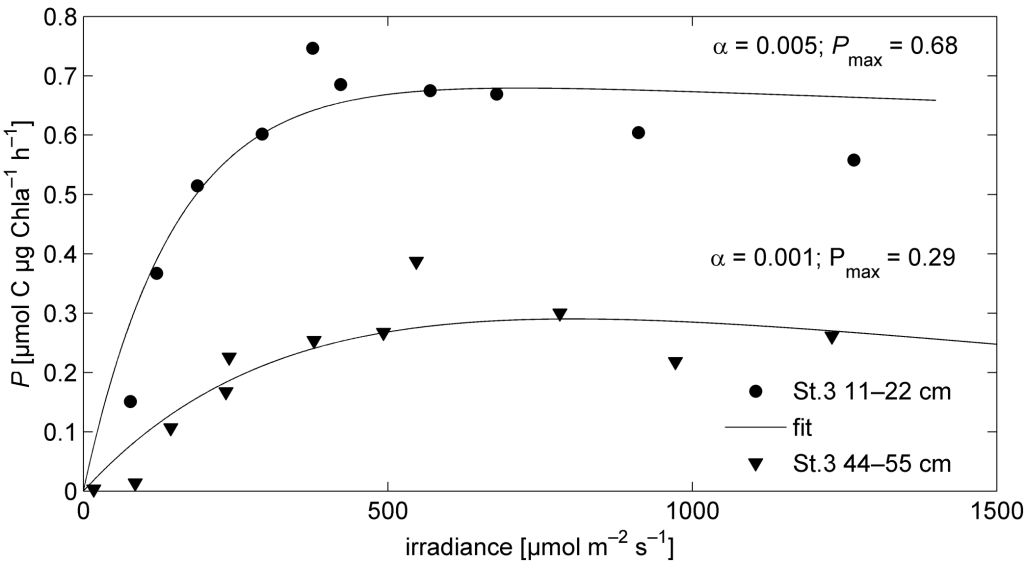

Figure 1

Examples of PI curves for melted sea ice.

PI curves, photosynthesis (P) versus irradiance, are shown for the bottom layer sample (triangles) and the layer of the second highest sample (circles) of fast ice at St.3 in the Gulf of Finland. The corresponding fits were obtained using MATLAB and used to calculate the photosynthetic efficiency α (shown), maximum photosynthesis, P_{max} (shown) and quantum yield of photosynthesis ϕ (not shown).

doi: 10.12952/journal.elementa.000121.f001

Computation of primary production

Our approach to calculate the primary production followed the absorption-based concept (Kiefer and Mitchell, 1983; Arrigo et al., 1991; Morel, 1991) and combines a radiative transfer model (Uusikivi et al., 2010), the measured absorption by algae, the measured maximum quantum yield and the measured photoadaptation parameter for primary production. The light field from the radiative transfer model was applied to the specific sampling site, depth and time. The light field was multiplied with the absorption by algae and the quantum yield of photosynthesis (as performed earlier by Lizotte and Priscu, 1994) to estimate the primary production at each depth in sea ice. The algorithm was applied separately for three runs, "St.3", "fast ice" and "GoF ice", and the parameterisation is summarised in Table 2. The "St.3" run uses the solar radiation and physical

Table 2. Parameterization of the different simulations

Simulation name[a]	mean E_d	a_{CDOM}	$a_{algae} + a_d$[b]	Snow depth (cm)	Snow composition	b[c]	ϕ^*_{max}[d]	E_k[d]
"GoF"	GoF	typical spectrum for GoF	mean of all stations	5	snow	140/4/2.6	0.009/0.006	191/217
"fastice"	St.3-specific	St.3-specific spectrum	mean of St.3 + St.4	8	snow	140/4/2.6	0.013/0.006	136/186
"St.3"	St.3-specific	St.3-specific spectrum	mean of St.3 + St.4	13	snow + slush	70/4/2.6	0.014/0.003	143/228
"St.3 depth"	St.3-specific	St.3-specific spectrum	mean of St.3 + St.4	10 [5]	snow + slush	120/4/2.6 [140/4/2.6]	0.014/0.003	143/228
"St.3 snow properties"	St.3-specific	St.3-specific spectrum	mean of St.3 + St.4	13	snow + slush [only snow]	70/4/2.6	0.014/0.003	143/228
"St.3 quantum yield"	St.3-specific	St.3-specific spectrum	mean of St.3 + St.4	13	snow + slush	70/4/2.6	0.0105/0.00225 [0.0175/0.00375]	143/228
"St.3 E_k"	St.3-specific	St.3-specific spectrum	mean of St.3 + St.4	13	snow + slush	70/4/2.6	0.014/0.003	107/171 [179/285]

[a]Parameterization of the different simulations: "GoF" describing the mean of all stations, "fastice" combines data from the two level fast ice stations, St.3 and St.4, and "St.3" is St.3 only. The simulations "St.3 depth", "St.3 snow properties", "St.3 quantum yield" and "St.3 E_k" applied two different values or sets of values where indicated (without brackets and within brackets).
[b]All values, numbers of replicates and coefficients of variation are given in Table 3.
[c]The scattering coefficient b is given for the three layers in the algorithm, "snow", "surface ice" and "bottom ice", separated by a backslash.
[d]The maximum quantum yield ϕ^*_{max} and the light saturation index E_k are given for the two ice layers of the algorithm, "surface ice" and "bottom ice", separated by a backslash.

doi: 10.12952/journal.elementa.000121.t002

and optical properties of ice and snow measured at St.3 to compute the primary production at each depth of the ice and to compare it to the primary production measured *in situ*. The absorption properties for the "St.3" run are specific for the bottom ice at St.3, but $a_{d,surface}$ and $a_{algae,\ surface}$ were calculated from the second layer of St.3 and the surface layers of St.4 because we were not completely successful in separating algal- and de-pigmented particles from the surface ice at St.3 (Table 3). The "St.3" run investigated methodological differences in primary production rates by comparing the calculated primary production rates to those measured *in situ* and to study the sensitivity of the algorithm. The "fast ice" run combined the input data for absorption properties, chlorophyll values and E_k values collected at St.3 and St.4 and, hence, represents the mean optical properties and mean primary production rates for level fast ice. The "GoF" run extended the input data towards other ice types to represent a typical case for different ice conditions in the Gulf of

Table 3. Measured concentrations of Chl *a*, absorption coefficients and spectral slopes of all ice layers at St.1 to St.4[a]

Station	Ice depth (cm)	Chl *a* (μg L^{-1})	a_{algae}	a^*_{algae}	a_d	a_{CDOM}	$S_{275–295}$	$S_{350–400}$	$S_{250–450}$	S_R ratio	$S_{380–730}$
St.1[b] drift ice	0–11	[0.81 ± 0.12]	-	-	-	[1.21/0.24]	[23.1]	[19.4]	[20.2]	[1.19]	[3.72]
	11–22	1.07 ± 0.08	0.09/0.06	0.08/0.05	0.31/0.16	0.89/0.15	23.7	20.8	20.7	1.14	7.13
	22–32	2.28 ± 0.00	0.12/0.08	0.05/0.04	0.32/0.19	1.03/0.21	23.1	19.4	20.0	1.19	5.47
	32–42	3.80 ± 0.30	0.09/0.09	0.02/0.02	0.54/0.32	1.00/0.20	22.6	19.2	19.5	1.18	5.63
	42–51.5	4.67 ± 0.47	0.13/0.13	0.03/0.03	0.28/0.18	0.77/0.15	23.2	19.9	19.8	1.17	4.74
	UIW	0.98 ± 0.06	0.1/0.07	0.1/0.07	0.22/0.13	3.88/0.69	22.8	19.7	19.7	1.16	2.70
St.2 deformed ice	0–15	2.24 ± 0.03	0.18/0.11	0.08/0.05	0.27/0.16	1.01/0.21	22.2	18.9	19.4	1.17	3.33
	15–30	4.48 ± 0.06	0.19/0.16	0.04/0.03	0.23/0.12	1.25/0.25	21.7	19.2	19.1	1.13	4.46
	30–47	5.64 ± 0.07	0.26/0.23	0.05/0.04	0.27/0.13	1.16/0.24	21.0	18.9	18.4	1.11	4.80
	47–65	4.39 ± 0.08	0.26/0.23	0.06/0.04	0.31/0.16	1.33/0.26	20.6	19.1	18.3	1.08	5.04
	65–82.5	2.43 ± 0.09	0.23/0.14	0.10/0.06	0.34/0.18	1.25/0.25	21.1	18.9	18.5	1.11	4.30
St.3[b] fast ice	0–11	[0.90 ± 0.01]	-	-	-	[1.74/0.29]	-	-	-	-	[3.36]
	11–22	13.8 ± 0.63	0.31/0.33	0.02/0.02	0.45/0.25	1.69/0.32	20.8	19.5	18.5	1.07	4.32
	22–33	3.32 ± 0.15	0.21/0.14	0.06/0.04	0.23/0.12	1.60/0.32	20.3	18.4	18.1	1.10	3.80
	33–44	1.26 ± 0.13	0.23/0.12	0.18/0.10	0.23/0.13	1.79/0.33	19.9	19.0	17.9	1.05	4.50
	44–55	2.34 ± 0.67	0.2/0.15	0.09/0.06	0.15/0.08	1.64/0.31	19.8	19.2	17.7	1.03	4.52
	UIW	0.50 ± 0.06	0.21/0.09	-	-	6.89/1.18	20.3	18.0	17.7	1.13	5.65
	slush	0.98 ± 0.55	0.14/0.09	0.12/0.09	0.12/0.09	5.31/0.93	20.3	18.7	18.1	1.09	3.20
St.4 fast ice	0–5	1.35 ± 0.68	0.15/0.07	0.11/0.05	0.31/0.23	0.88/0.11	24.4	23.4	21.7	1.04	3.47
	5–10	3.90 ± 0.66	0.15/0.15	0.04/0.04	0.50/0.38	0.53/0.05	23.9	24.8	20.5	0.96	3.26
	10–26	6.83 ± 1.48	0.06/0.15	0.01/0.02	0.59/0.392	0.65/0.08	23.2	21.9	20.3	1.06	3.97
	26–36	6.17 ± 1.63	0.37/0.26	0.06/0.04	0.11/0.04	1.77/0.27	20.6	20.3	18.4	1.01	10.91
	UIW	0.86 ± 0.20	0.20/0.07	0.23/0.08	0.28/0.09	6.90/1.22	19.4	18.9	17.6	1.03	9.71
Mean, fast ice	**surface, n = 4**	**6.47** ± 5.4	**0.17/0.17**	**0.04/0.03**	**0.46/0.31**	**0.94/0.14**	**23.1**	**22.4**	**20.2**	**1.03**	**3.76**
	bottom, n = 4	**3.27** ± 2.1	**0.25/0.17**	**0.09/0.06**	**0.18/0.09**	**1.70/0.31**	**20.2**	**19.2**	**18.0**	**1.05**	**5.93**
Mean, total	**surface, n = 7**	**4.81** ± 4.4	**0.16/0.15**	**0.06/0.04**	**0.38/0.24**	**0.99/0.16**	**23.8**	**21.2**	**20.0**	**1.08**	**4.28**
	bottom, n = 10	**3.63** ± 1.6	**0.21/0.16**	**0.07/0.05**	**0.28/0.15**	**1.33/0.25**	**21.2**	**19.2**	**18.7**	**1.10**	**5.37**
	UIW, n = 3	**0.78** ± 0.3	-	**0.17/0.07**	**0.25/0.11**	**5.39/0.95**	**21.1**	**18.9**	**18.6**	**1.09**	**6.21**

[a]Abbreviations [and units]: depth at each station [cm] with n = 3–5; Chl *a* = chlorophyll *a* [μg L^{-1}] with the standard deviation for n = 3; a_{algae} = absorption of algae-related particles at 350 and 443 nm [m^{-1}]; a^*_{algae} = absorption of algae-related particles at 350 and 443 nm relative to Chl *a* [m^2 mg Chl a^{-1}]; a_d = absorption of de-pigmented particles at 350 and 443 nm [m^{-1}]; a_{CDOM} at 350 and 443 nm [m^{-1}]; $S_{275–295}$ = spectral slope coefficient of CDOM for the 275–295 nm range [μm^{-1}]; $S_{350–400}$ = spectral slope coefficient of CDOM for the 350–400 nm range [μm^{-1}]; $S_{250–450}$ = spectral slope coefficient of CDOM for the 250–450 nm range [μm^{-1}]; SR ratio = ratio between the spectral slope of CDOM of $S_{275–295}$ to $S_{350–400}$; $S_{380–730}$ = spectral slope coefficient to describe de-pigmented matter for the 380–730 nm range [μm^{-1}]; dash indicates no data available.

[b]Samples in brackets were not included in the calculation of mean values that were used as input parameters for "fast ice run" ("fast ice" of surface, bottom ice) and the "GoF ice run" ("total" of surface, bottom and UIW) of the algorithm.

doi: 10.12952/journal.elementa.000121.t003

Finland by also including absorption data, chlorophyll values and E_k values of the drift ice station (St.1) and the deformed ice station (St.2). For the "GoF" run, the typical solar radiation at 60° N for mid-March was applied as calculated earlier by Kuivikko et al. (2007). The snow and ice structure for the "GoF" run and the "fastice" run were assumed to be similar to those observed at St.3 with the upper two layers being surface ice and the lower three layers being bottom ice. Absorptions were calculated for both runs ("GoF" and "fastice") without the surface layer samples at St.1 and St.3 because a_{algae} was in doubt. The values used for the calculations are shown in Tables 2 and 3. The effect of changing snow depth and properties (E_k and ϕ_{max}^*) on the calculated primary production was tested ("St.3 test") with the range of tested parameters given in Table 2.

Our radiative transfer model adapted from Uusikivi et al. (2010) consists of three layers. The uppermost layer is comprised of snow and slush. The model separates solid sea ice into a surface layer consisting of small randomly oriented ice crystals with meteoric water (called surface ice) and a bottom layer consisting of columnar ice crystals formed from seawater (called bottom ice). The radiative transfer model used the spectral quantum irradiance incident to the surface of snow (E_d) during sampling at St.3 and PAR derived from the measured solar radiation at 1-min intervals on March 14–15 at St.3 simultaneously with the measurement of primary production *in situ*. For GoF ice, the radiative transfer model used the typical spectral plane incident irradiance in the middle of May at 60° N during a typical daily distribution at that time of year (Kuivikko et al., 2007).

The scattering coefficient *b* was obtained using albedos and transmissions of a two-stream radiative transfer model (Perovich, 1990) by finding the best fit between the calculated and measured values (Uusikivi et al., 2010). The best fit for *b* was defined by minimising root-mean-square error between modelled and observed albedo and transmittance using a range of values obtained from the literature (Perovich, 1990). The *b* value for the ice layer without snow was determined first, then used to fit the snow layer to the measured albedo and transmittance with snow cover on ice.

To convert the scalar irradiance absorbed by algae in the ice to fixed carbon by photosynthesis, the maximum quantum yield of photosynthesis, ϕ^*_{max}, was calculated according to Sakshaug et al. (1991):

$$\phi^*_{max} = \alpha(\bar{a}^*)^{-1} \tag{7}$$

where α is the photosynthetic efficiency derived from the PI curves and $\bar{a}^*$ is a spectrally-weighted absorption coefficient by a_{algae} in the PI incubator. Parameter $\bar{a}^*$ was derived according to:

$$\bar{a}^* = \sum_{400}^{700}[E_d(\lambda)\, a_{algae}(\lambda)]\,[\sum_{400}^{700} E_d(\lambda)]^{-1} \tag{8}$$

where $a_{algae}(\lambda)$ refers to a measured value for each individual sample and $E_d(\lambda)$ is the spectral irradiance of the PI incubator derived from Raateoja et al. (2004), who used the same PI incubator.

The photosynthesis rate (P) at depth z across the thickness of ice at a 1-cm depth interval was calculated according to Kirk (1994) by:

$$P = T_{corr}\phi\int_{400}^{700}[E_0 a_{algae}(\lambda)]d\lambda \tag{9}$$

with ϕ calculated after Eppley (1972) and Bidigare et al. (1992) by:

$$\phi = \phi^*_{max}\frac{E_k}{E_0}[1 - e^{-\frac{E_0}{E_k}}] \tag{10}$$

where E_0 is the spectral scalar irradiance (mol photons m^{-2} s^{-1} nm^{-1}) integrated over the PAR range at each depth derived from the radiative transfer model, $a_{algae}(\lambda)$ is the measured absorption coefficient of algae (m^{-1} nm^{-1}) expressed as a mean value calculated separately for the surface or the bottom layers of ice, ϕ^*_{max} is the measured maximum quantum efficiency for photosynthesis (mol C mol photons^{-1}) as defined by Eq. 7, and T_{corr} is a temperature correction factor. The effect of the temperature difference on P (T_{corr}) between the PI measurements and *in situ* measurements was calculated by:

$$T_{corr} = \exp[-r_\mu(T_{PI} - T_{insitu})] \tag{11}$$

where r_μ = 0.0633 as the rate constant to determine the temperature sensitivity of the growth rate of phytoplankton acclimated to temperatures > 2 °C (Arrigo and Sullivan, 1994). T_{PI} is the temperature during the PI incubations (4 °C) and T_{insitu} is the measured ice temperature directly after coring (Table 1).

The primary production to biomass ratio was calculated by dividing P (Eq. 9) with the concentration of Chl *a*.

Sensitivity of the algorithm

The input parameters to the "St.3" run were varied to describe the effect on the light spectrum and the primary production in the different layers (Table 2). Snow depth is one of the main parameters controlling the

light conditions in ice and, hence, also controlling primary production. The 13-cm snow and slush layer at St.3 was reduced to 10 cm (75%) and 5 cm (as the typical snow layer in the whole dataset). The effect of the composition of snow, either snow of the density 0.26 g cm^{-3} or a mix of snow with slush, on the light field and the resulting primary production was tested. Furthermore, the sensitivity of the algorithm to the E_k value and ϕ_{max} was investigated by reducing and enhancing both parameters to 75% and 125% in the algorithm, respectively. For all test runs, only the scattering of snow was adjusted to fit the transmitted light. All other parameters remained constant during the different runs.

Results

Absorption coefficients

The absorption coefficients of CDOM, de-pigmented particles and phytoplankton-related particles are presented in Table 3 and Figures S1–S3. The mean of the two fast ice stations ("fast ice") and the mean of all four stations in the GoF ("GoF ice") are shown in Figure 2. The separation of the algal-related particles at the surface layer of St.3 was difficult due to the low concentration in algae compared to a_d values resulting in an unrealistic spectrum (Figure S2). The surface layer of St.3 was therefore excluded from the mean value calculations and the input data for the algorithm. The variation in algae-related particles (Figure 2e–h, Table 3) of sea ice was high among the stations and the depths. Highest values for $a_{algae,350}$ were measured in the surface layers of the drift ice station and in one of the fast ice stations, but also in the bottom layer of the other fast ice station (Table 3). After normalisation to Chl *a*, all sea-ice stations have highest $a_{algae,350}$ and

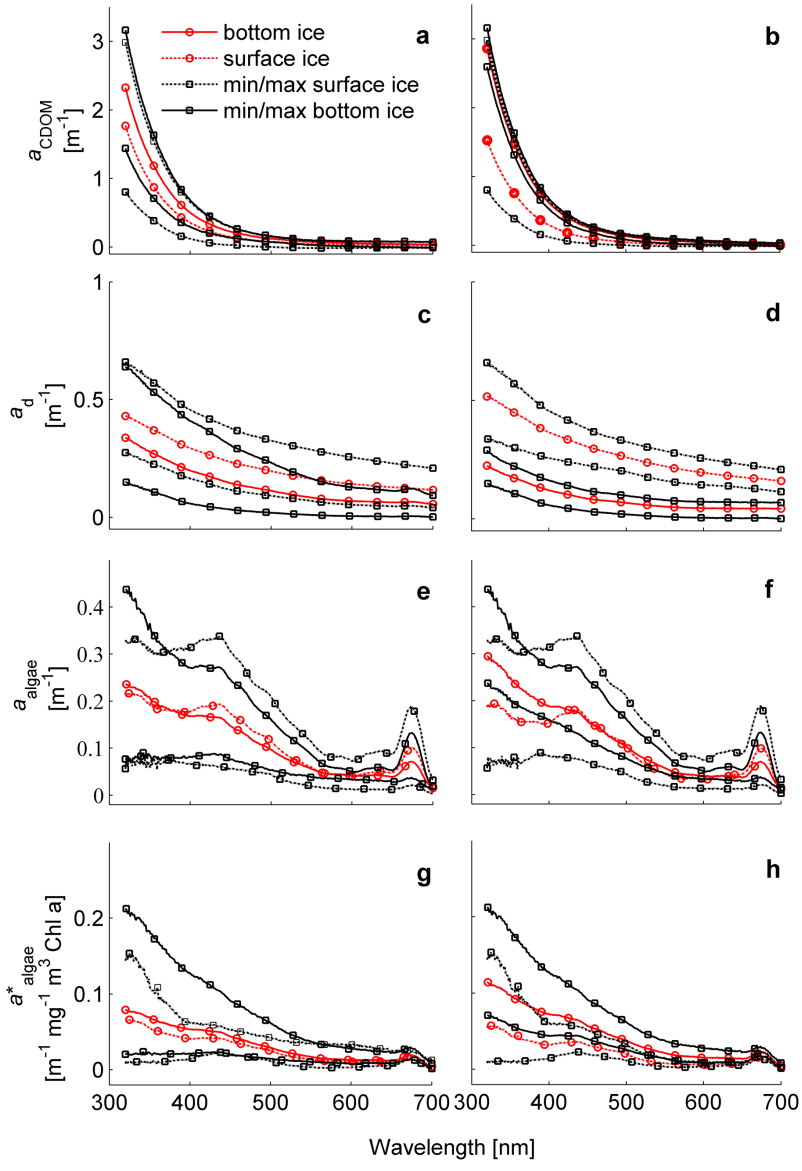

Figure 2

Absorption spectra of CDOM, de-pigmented particles and algae for melted sea ice.

The spectra of absorption coefficients are shown for CDOM (a_{CDOM}, panels a and b), de-pigmented particles (a_d, panels c and d), algae (a_{algae}, panels e and f) and algae normalized to Chl *a* (a^*_{algae}, panels g and h). The mean coefficients (red lines) and their minimal and maximal values (black lines) are shown for surface ice (dotted lines) and bottom ice (solid lines). In panels a, c, e and g, the mean absorption properties are derived from all stations; in panels b, d, f and h, the mean values are those for fast ice only (St.3 and St.4). Please note the different scales for the absorption coefficients.

doi: 10.12952/journal.elementa.000121.f002

$a_{algae,443}$ in the surface layers, but also in the UIW (Figure 2g and h, Table 3). The value for a_d is also different at every station, with highest values at the drift ice station and the surface layer of one of the fast ice stations (Figure 2c and d, Table 3). All stations except the deformed fast ice station (St.2) have lowest a_d in the bottom layers. The spectral slope of a_d, $S_{380–730,}$ ranged between 3.33 μm^{-1} in the surface ice of St.2 and 10.91 μm^{-1} in the bottom ice of St.4 (Table 3). The variability was lower for St.1 to St.3, ranging from 3.33 to 7.13 μm^{-1} without a significant difference between stations or between the surface and bottom layers (independent T-test, SPSS; $p \leq 0.05$) than for St.4, which was closest to the coastline. Values for $S_{380–730}$ of a_d were lowest in slush, containing seawater and snow, at St.3.

The $a_{CDOM}(\lambda)$ (Figure 2a and b, Table 3) resulted in typical CDOM spectra that varied between 0.5 and 1.8 m^{-1} in sea ice and between 3.9 and 6.9 m^{-1} in UIW at 350 nm. At 443 nm, $a_{CDOM}(\lambda)$ varied between 0.05 and 0.33 m^{-1} in sea ice and was lower in ice than in UIW. The variation in $a_{CDOM}(\lambda)$ did not indicate a consistent pattern with depth or among stations. The two fast ice stations had highest $a_{CDOM}(\lambda)$ in the bottom layer and lowest in the surface layer, while the opposite was found at the drift ice station. The deformed ice station showed lowest variability among layers. The $a_{CDOM,443}$ exhibited a clear difference between the two fast ice stations, with lowest values in the middle layers of St.4 but highest values at St.3. While the vertical variability of $a_{CDOM}(\lambda)$ was highest in the fast ice stations, S_λ and S_R of CDOM varied most at the drift ice and deformed ice stations with highest slopes in the upper layers. In a nutshell, these absorption measurements of Baltic Sea ice and UIW showed a high variability that was strongly influenced by the history of the ice and its individual biogeochemical conditions.

The spectral shape for a_{algae} and a^*_{algae} (Figure 2e–h) was similar for surface and bottom ice at all stations showing peaks at approximately 420 to 470 nm and 600 to 700 nm, which represent the mix of photosynthetic and photo-protective pigments. The absorption by algal pigments (a_{algae}) at 350 and 443 nm (Table 3) was higher in the bottom layers than the surface layers at all stations except St.3 (fast ice). In contrast, a^*_{algae} was higher in the surface layers than the bottom layers, except at St.3. The absorption value for a_{algae} exceeded a_{CDOM} at $\lambda >$ ca. 500 nm and included typical Soret bands of Chl *a* (Figure 2e and f). Nutrient concentrations varied among the stations, with lowest concentrations generally in the level fast ice station 4 and highest concentrations at the other fast ice stations (Table S1). The relative concentrations of the different nutrients varied inconsistently among stations and vertical depths.

Albedo, transmittance and scattering coefficients

The spectral albedo measured over an undisturbed snow cover at St.3 ranged from 0.93 to 0.94 (Figure 3a) and the transmittance across the undisturbed snow and ice cover was 0.02–0.03 (Figure 3b). The scattering coefficient, *b*, was 140 m^{-1} in the layer above the solid ice (snow and slush), 4 m^{-1} in surface ice, and 2.6 m^{-1} in the bottom ice of St.3 (Table 1), when determined by a two-stream radiative transfer model with the measured (Figure 2b, d, f, and h) and estimated (Eq. 1 and 2) absorption coefficients. The modelled albedo (Figure 3a) and transmittance (Figure 3b) were fitted to the measured ones (Figure 3a and b) by altering the scattering coefficients of ice.

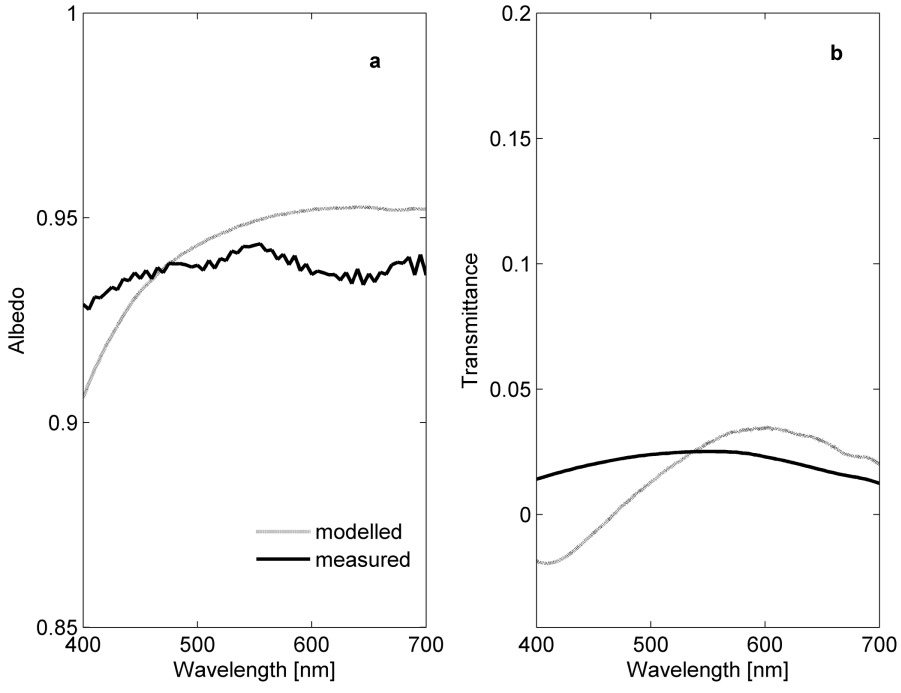

Figure 3

Measured versus modelled albedo and transmittances.

Spectral albedo (a) and transmittance (b) measured at St.3 fast ice (black line) and modelled for fast ice (grey line) in the Gulf of Finland.

doi: 10.12952/journal.elementa.000121.f003

Light available for photosynthesis in sea ice

In order to evaluate the total amount of solar radiation available for algae in sea ice during a 24-h period, the daily modelled scalar irradiance for PAR (E_0) was presented for each depth for "St.3", "fast ice" and "GoF ice" (Figure 4). A 5-cm snow layer decreased E_0 at the surface of snow (E_0 z = 5 cm) to 16.2% in the uppermost centimeter of surface ice at St.3. Thicker snow layers of 10 cm and 13 cm reduced the light that reached the ice surface to 7.3% and 6.4%, respectively. The 5-cm snow layer on top of the "GoF ice" (mean of all stations) reduced PAR by 81.1% (Figure 4). The surface ice further attenuated PAR to less than 10% under 5-cm deep snow, and to 4.5% under 13-cm deep snow. The attenuation of E_0 was spectrally relatively flat both by snow and ice without remarkable spectral shaping for light available for photosynthesis (spectra not shown). PAR at the ice bottom was 0.4, 0.9 and 0.6 mol photons m^{-2} d^{-1} at St.3, fast ice and GoF ice, respectively.

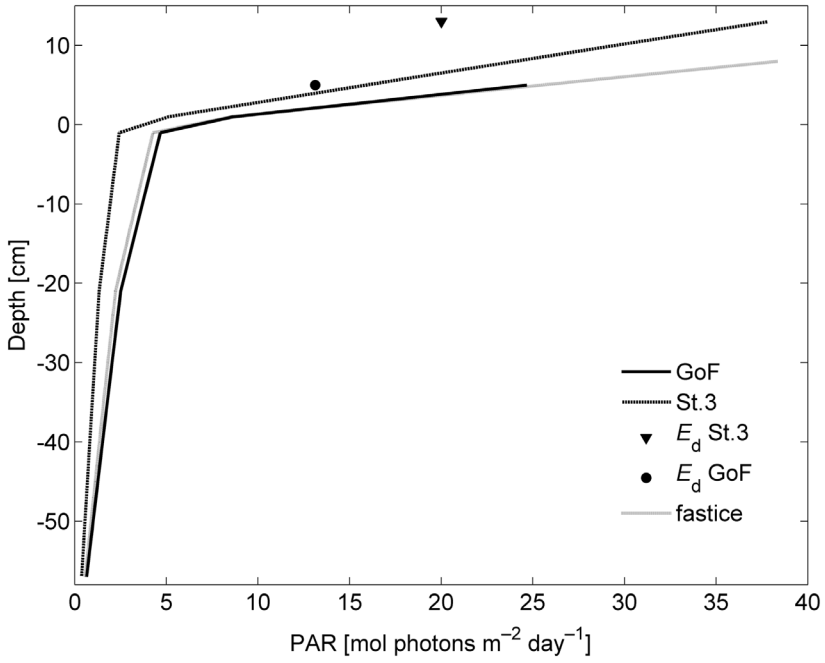

Figure 4

Modelled and measured photosynthetically active irradiances over the snow and ice surface.

The modelled photosynthetically active radiation (PAR) is shown throughout the snow and ice layers at St.3 (dotted line), for fast ice stations (grey line), and for typical conditions in March (GoF ice, solid black line). Measured plane downwelling irradiance (E_d) over the surface is shown as a triangle (13-cm snow depth) at St.3 or a circle (5 cm snow depth) for typical conditions at these Gulf of Finland (GoF) stations in March.

doi: 10.12952/journal.elementa.000121.f004

Primary production

In the photosynthesis-irradiance experiments, maximum photosynthetic rate (P_m) varied between 0.31 and 1.07 µg C µg Chl a^{-1} h^{-1}, with highest values close to the interface between surface and bottom ice (Table 4). Stations 1 and 2 also exhibited highest P_m values in the middle layers (Table 4). Maximum light utilisation coefficients (α) ranged from 0.001 to 0.010 without a depth-dependent distribution (Table 4). Maximum values in ā* were found in the surface layers at St.1, middle layers of St.3 and in the bottom layer of the deformed ice at St.2, with an overall variation from 0.007 to 0.031 (Table 4). Maximum quantum yields for C fixation (ϕ^*_{max}) ranged between 0.002 and 0.016 mol C mol photons^{-1} and again with high ϕ^*_{max} in the 11–22 cm layer of St.3, while St.1 and St.2 exhibited highest values in the middle layers (Table 4). The mean ϕ^*_{max} for surface ice from all stations (0.009 mol C mol photons^{-1}) was not significantly different from the mean value for all bottom ice (0.006 mol C mol photons^{-1}; independent T-test, SPSS; $p \leq 0.05$).

At St.3 the quantum yield for carbon fixation (ϕ), calculated using Eq. 9, was 0.009 mol C mol photons^{-1} at the maximum light level and 0.012 mol C mol photons^{-1} at the minimum light level in surface ice. In bottom ice, ϕ ranged between 0.005 and 0.006 mol C mol photons^{-1}, respectively. In the "GoF" run of the algorithm, ϕ ranged between 0.006 and 0.009 mol C mol photons^{-1} in surface ice and between 0.004 and 0.006 mol C mol photons^{-1} in bottom ice at highest and lowest light levels, respectively. The difference in ϕ between the surface and bottom layers of all stations was significant (independent T-test, SPSS; $p \leq 0.05$), with the mean ϕ of surface ice and bottom ice being 0.007 and 0.005 mol C mol photons^{-1}, respectively (SD < 0.001).

The calculated primary production integrated over a day (P) in the fast ice St.3 ranged from 0.3 (depth of 56 cm) to 5.4 (depth of 1 cm) mg C m^{-3} d^{-1} (Figure 5a). Chl a-normalised P (P^*) varied between 0.1 and 0.8 mg C mg Chl a^{-1} d^{-1} at St.3 (Figure 5b). When the algorithm was applied to the mean conditions of mid-March in the Gulf of Finland ("GoF" run), P ranged from 2.3 at the bottom to 42.4 mg C m^{-3} d^{-1} at the surface of the ice (Figure 5a) and a corresponding P^* from 0.6 to 8.8 mg C mg Chl a^{-1} d^{-1} (Figure 5b). In the surface ice of St.3, a maximum P of 0.22 µg C m^{-3} s^{-1} and a maximum P^* of 0.034 µg C µg Chl a^{-1} s^{-1}

Table 4. Photobiological variables calculated from measured parameters[a]

Station	Ice depth (cm)	ã*	α	P_m	R^2	E_k	ϕ^*_{max}	$P_{in\ situ}$
St. 1 drift ice	0–11	-	0.002	0.618	0.75	301	-	0.427
	11–22	0.031	0.003	0.416	0.75	137	0.002	0.478
	22–32	0.018	0.003	0.782	0.92	271	0.004	0.453
	32–42	0.011	0.006	0.605	0.92	108	0.012	0.354
	42–51.5	0.011	0.002	0.499	0.89	328	0.003	0.237
St. 2 deformed ice	0–15	0.017	0.002	0.533	0.62	355	0.002	-
	15–30	0.012	0.003	0.87	0.93	298	0.006	-
	30–47	0.016	0.007	0.94	0.98	138	0.010	-
	47–65	0.013	0.002	0.88	0.67	344	0.004	-
	65–82.5	0.023	0.002	0.43	0.33	234	0.002	-
St. 3 fast ice	0–11	-	-	-	-	-	-	0.549
	11–22	0.008	0.005	0.68	0.88	143	0.014	0.746
	22–33	0.016	0.001	0.52	0.88	349	0.002	0.386
	33–44	0.027	0.005	0.40	0.72	75	0.005	0.276
	44–55	0.015	0.001	0.29	0.89	259	0.002	0.254
St. 4[b] fast ice	0–5	0.015	0.005	0.66	0.74	139	0.008	-
	5–10	0.012	0.005	0.72	0.82	149	0.010	-
	10–25	0.007	0.006	0.72	0.92	114	0.020	-
	25–35	0.014	0.010	0.65	0.92	62	0.016	-
Mean, fast ice	**surface, n = 4**	**0.010**	**0.005**	**0.68**	-	**136**	**0.013**	**0.648**
	bottom, n = 4	**0.018**	**0.005**	**0.40**	-	**186**	**0.006**	**0.305**
Mean, total	**surface, n = 7**	**0.014**	**0.004**	**0.63**	-	**191**	**0.009**	**0.550**
	bottom, n = 10	**0.016**	**0.004**	**0.58**	-	**217**	**0.006**	**0.327**

[a]Abbreviations [and units]: depth at each station [cm] with n = 3–5; ã* = Chl *a*-normalized spectrally-weighted absorption coefficient by a_{algae} [m^2 mg Chl a^{-1}]; α = maximum light utilisation coefficient [µg C µg Chl a^{-1} h^{-1} (µmol photons m^{-2} $s^{-1})^{-1}$]; P_m= maximum photosynthetic rate [µg C µg Chl a^{-1} h^{-1}]; R^2 = coefficient of determination for the fit of data to Eq. 6; E_k = light saturation index [µmol photons m^{-2} s^{-1}]; ϕ^*_{max} = maximum quantum yield [mol C mol photons^{-1}]; P_{insitu} = photosynthesis measured *in situ* [mg C mg Chl a^{-1} d^{-1}]; dash indicates no data available.

[b]Data from Enberg et al. (2015)

doi: 10.12952/journal.elementa.000121.t004

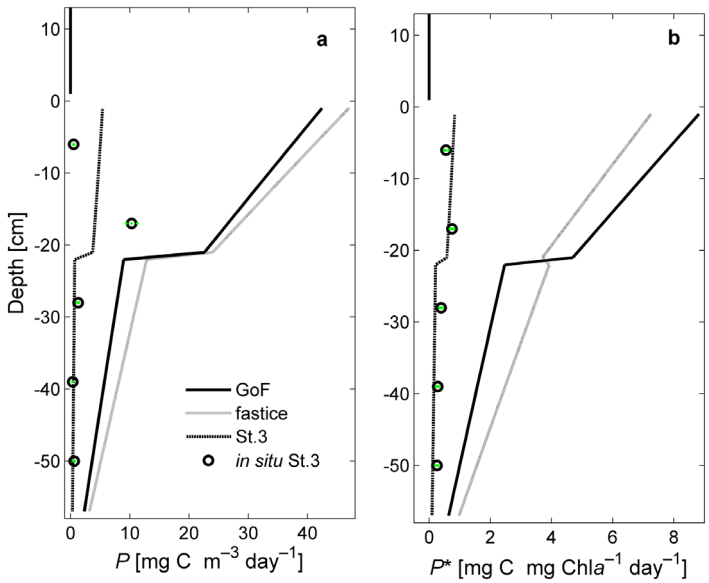

Figure 5

Calculated and *in situ* measurements of primary production rates.

The calculated daily rates of primary production, *P*, and primary production normalized to Chl a, *P**, are presented in panels a and b, respectively, over the entire ice depth for the means of St.3 (dotted line), the fast ice stations (grey line), and all of the Gulf of Finland GoF stations (black line). These calculated results are shown in comparison to the mean values of *in situ* measurements of *P* and *P** for all 5 ice layers (black circles), where the standard deviation among replicates is shown in green. Note that samples from all layers were incubated *in situ* at a depth of 10 cm and that no^{14}C measurements were made on snow; the vertical black lines above 0 depth assume negligible *P* in the snow.

doi: 10.12952/journal.elementa.000121.f005

were calculated for the 24-h incubation period. The maximum P in the columnar ice was 0.15 mg C m^{-3} d^{-1} with a corresponding maximum P^* of 0.024 µg C µg Chl a^{-1} s^{-1}. At the bottommost centimeter at St.3, P was at maximum 0.012 µg C m^{-3} s^{-1} and P^*, 0.004 µg C µg Chl a^{-1} s^{-1}. The maximum P values for typical conditions in the Gulf of Finland in mid-March were estimated to be 1.67 µg C m^{-3} s^{-1} in the surface, 0.35 µg C m^{-3} s^{-1} in the bottom ice layer and 0.09 µg C m^{-3} s^{-1} at the bottommost centimeter of the ice. Corresponding P^* values were 0.35, 0.10 and 0.03 µg C µg Chl a^{-1} s^{-1} at these three depths, respectively.

The P measured *in situ* was lower than the calculated P in the uppermost layer, but the opposite was found in the bottom layer (Figure 5a and b; Table 3). Calculated P values agreed better with *in situ* measurements for P^* than for P (Figure 5b).

The results of the sensitivity study testing the effect of the parameters snow depth, snow composition, E_k and ϕ_{max} on the calculated primary production rates are shown in Figure 6. A 3-cm decrease in snow depth resulted in a 14% increase in PAR and an increase in P of up to 200%. The quantum yield also clearly affected the primary production (Figure 6d), whereas the change in E_k by 25% (Figure 6c) did not result in distinguishable differences.

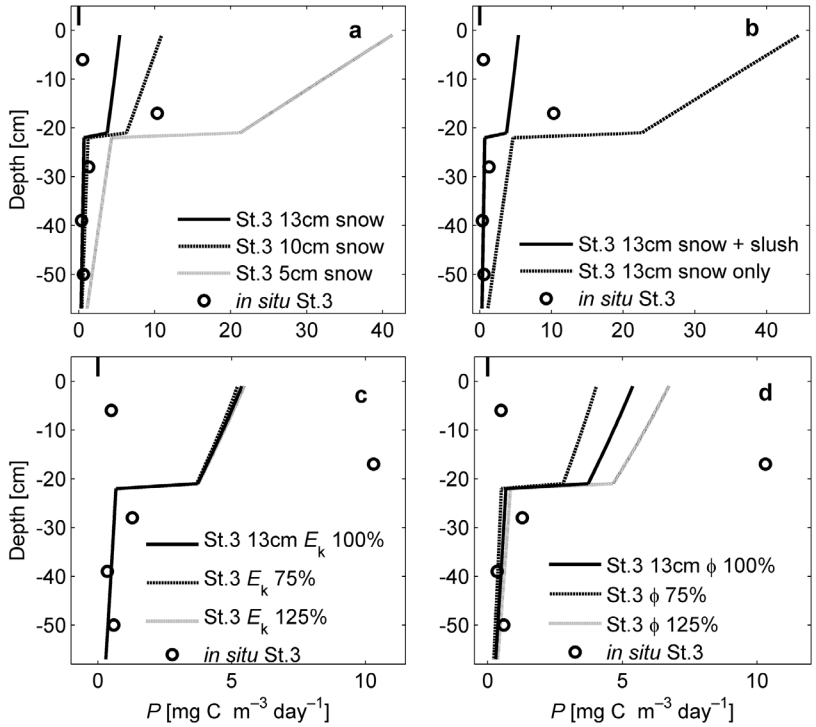

Figure 6

Sensitivity tests of the applied algorithm.

The sensitivity tests for the algorithm applied in this study addressed the effects of snow depth (a), snow properties (b), light saturation index, E_k (c) and maximum quantum yield, ϕ_{max} (d) on calculated primary production rates in the ice at St.3. Primary production rates based on *in situ* measurements (circles) are provided for comparison (see Figure 5). Definitions of lines used in each panel are provided on the figure; detailed parameter settings are given in Table 2.

doi: 10.12952/journal.elementa.000121.f006

Discussion

Bio-optical parameters

The presented data set combines different ice types of the Baltic Sea and covers the range of sea-ice bio-optical properties in the Gulf of Finland. The ice thickness at St.3 consisted of 36% surface ice (granular ice) and 64% bottom ice (columnar ice), which is similar to the findings of Granskog (2004).

The measured absorption coefficients of CDOM from 350 nm to 380 nm agree with earlier measurements in Baltic Sea ice that varied between 0.2 and 2 m^{-1} (Ehn et al., 2004; Stedmon et al., 2007; Uusikivi et al., 2010; Müller et al., 2011). Also, at the blue absorption (443 nm), a_{CDOM} results from all stations are similar to studies in the Arctic Ocean (Matsuoka et al., 2009) and in European waters (Babin et al., 2003). Only a few earlier studies have presented particle absorption in sea ice from the Arctic or Baltic Sea; our results are similar in spectral shape and absorption intensity to those presented earlier (Uusikivi et al., 2010; Ehn et al., 2008a). Chlorophyll *a*-specific absorption by phytoplankton (a^*_{algae}) was reported in other studies to be below 0.07 m^2 mg Chl a^{-1} at 350 nm in interior and bottom ice layers (Mundy et al., 2011) and below 0.07 m^2 mg Chl a^{-1} at 443 nm at the bottom of Arctic sea ice (Ehn et al., 2008b). Our results are similar: for the bottom layers of ice at all stations, the mean values for a^*_{algae} at 350 and 443 nm were 0.07 and 0.05 m^2 mg Chl a^{-1}, respectively, while the mean values for only the fast ice stations were 0.09 and 0.06 m^2 mg Chl a^{-1}, respectively (Table 3). In addition to earlier studies, our study also provides optical properties in the upper layers of the ice and in UIW and slush.

In the case of de-pigmented particles, surface layers were characterised by different absorption properties than bottom layers at the fast ice stations, with higher a_d in the surface layers than the bottom layers (Table 3). The spectral slope, $S_{380–730}$, which has been used to describe the optical properties of de-pigmented particles, differed significantly between surface and bottom ice at St.4 (independent T-test, SPSS; $p \leq 0.05$; Table 3) with $S_{380–730}$ of UIW and bottom ice being close to $S_{380–730}$ reported for European waters (Babin et al., 2003). At all other stations, $S_{380–730}$ in ice, slush and UIW was below the reported average of 12.3 μm^{-1} (Babin et al., 2003). Stations 1–3 are close to soot sources on the eastern side of the GoF with higher atmospheric depositions compared to the western GoF (Jalkanen et al., 2000; Hyvärinen et al., 2011; Piiparinen et al., 2015). Atmospheric depositions of soot decrease $S_{380–730}$ because soot absorbs in the infra-red wavelength range (Hyvärinen et al., 2011). The enhanced atmospheric deposition by power plants and other soot sources (e.g., heavy ship traffic during winter season in the GoF; Table 8 in Hänninen et al., 2002) can explain low values of $S_{380–730}$ close to soot sources. In wintertime, when atmospheric depositions are at their maximum, the deposition accumulates on ice over the wintertime and can be seen in the optics of the Baltic Sea ice.

The albedo measured at St.3 is similar to the albedo reported for Baltic Sea ice by Pirazzini (2006) and for Arctic sea ice by Nicolaus (2010a, 2010b), but higher than in Ehn et al. (2004) and Uusikivi et al. (2010) as the snow thickness in the latter data sets were lower. This comparison indicates that St.3 represents typical Baltic Sea conditions but with comparably low light levels within the ice due to the thick snow cover.

The measured transmittance at St.3 can be compared to Baltic Sea studies, though they involved much thinner ice layers: Ehn et al. (2004) reported transmittances of 0.3–0.7 for ice no more than 28 cm thick in March and April. Uusikivi et al. (2010) also measured higher transmittance than our study because of the thinner ice layer (transmittance of 0.5 for 37 cm ice thickness), lower albedo and missing snow cover. Compared to transmittance through Arctic sea ice our results are similar even though the ice thickness was greater: Ehn et al. (2008b) measured a transmittance below 0.04 in sea ice of more than 1.7 m ice thickness and Nicolaus et al. (2010b) reported transmittances below 0.03 under sea ice of 1.4 m depth. Again, this comparison indicates that our sampling site for the light measurements (St.3) is an example for ice with low light conditions. Light measurements at our other sampling sites (St.1, St.2, St.4) would probably have resulted in lower albedos and higher transmittances due to the smaller snow depths and missing slush layers.

The scattering coefficient b was determined using the present radiative transfer model to fit the daily measured mean optical properties. For snow, b was 140 m^{-1}, which is close to that for wet snow reported by Perovich (1990). The scattering coefficient for surface ice of 4 m^{-1} is lower than reported by Uusikivi et al. (2010) for Baltic Sea granular ice, where b was 430 m^{-1}, but similar to b of 2.5 m^{-1} defined for "white ice interior" by Perovich (1990) for Arctic sea ice. Columnar ice scattered in our model with b of 2.6 m^{-1}, which is again lower than reported by Uusikivi et al. (2010), where b was 13 m^{-1} for columnar ice. For the model runs with thicker snow layers, the values for b were again adjusted to get the best possible fit between modelled and measured transmittance and albedo (Table 2). For St.3 with 13 cm snow and slush, the best fit resulted in negative values for the modelled transmittance in the spectral range below 450 nm because of the high a_{CDOM} in slush. This result indicates that the spectral range in the algorithm should also change with depth in the future. In the present version of the algorithm, absorption in the short-wavelength range of the algorithm is too high and results in the underestimation of E_0 (at this range) and of the primary production rates.

Our radiative transfer model calculates the light available for photosynthesis (PAR range) in 1-cm increments (Figure 4) for the entire ice column. The maximum mean modelled downwelling quantum irradiances for PAR ($E_{o,PAR}$, integrated over the 400 to 700 nm range) at noon were 101 and 54 µmol photons m^{-2} s^{-1} in the top of surface and bottom ice at St.3, respectively, and 185 and 97 µmol photons m^{-2} s^{-1} in GoF ice, respectively. $E_{0,PAR}$ is lower in both of these ice types than the values in Uusikivi et al. (2010), who reported 629, 420 and 370 µmol photons m^{-2} s^{-1} for the surface, middle and bottom layers of Baltic Sea ice. The measured quantum irradiance for $E_{d,PAR}$ at the surface of snow was 1465 and 977 µmol photons m^{-2} s^{-1} at St.3 and GoF, respectively, and 709 µmol photons m^{-2} s^{-1} in the study by Uusikivi et al. (2010) on the ice surface without snow cover. In our present study, the 5 cm thick snow cover alone reduced E_o by more than 80%, which agrees with transmittance measurements on snow by Järvinen and Leppäranta (2011). The high attenuation of light by snow highlights the importance of careful and accurate measurements on snow and slush additionally to the ice optical properties to describe and model sea ice.

Primary production

Photosynthetic parameters derived from PI curves are in the same range as earlier studies on Baltic Sea ice: the mean photosynthetic efficiency α (mg C mg Chla^{-1} h^{-1} [µmol photons m^{-2} s^{-1}]$^{-1}$) was 0.004 in bottom and surface ice in our present study and hence is very similar to α values reported for sea ice from the Bothnian Bay in Piiparinen et al. (2010) with 0.004, 0.0046 and 0.0048 µg C µg Chl a^{-1} h^{-1} [µmol photons m^{-2} s^{-1}]$^{-1}$ in top, middle and bottom layers, respectively. For the same location, Rintala et al. (2010) reported α values ranging between 0.001 and 0.032 in different layers of sea ice in the beginning of March.

In Baltic Sea ice, reported maximum photosynthesis rates per unit Chl a (P_m) were below 1.29 µg C $µg^{-1}$ Chl a h^{-1}, measured from incubation experiments (Rintala et al., 2010). The results of our present

study agree well with this report, as the mean P_m of all stations in surface ice was 0.63 μg C μg Chl a^{-1} h^{-1} and 0.58 μg C μg Chl a^{-1} h^{-1} in bottom ice.

According to Kaartokallio et al. (2007), primary production in Baltic Sea ice, obtained from incubation experiments at 80 μmol photons m^{-2} s^{-1}, was 0.9 μg C μg Chl a^{-1} h^{-1}. If the algorithm in our study is applied to the same light level of 80 μmol photons m^{-2} s^{-1} as in Kaartokallio et al. (2007), then P^*(fastice) is lower, with a value of 0.3 μg C μg Chl a^{-1} h^{-1}, and P^*(St.3) is 0.1 μg C μg Chl a^{-1} h^{-1}.

A direct comparison of results from several different studies is important for drawing general conclusions. Combining measured results with modelling, as done here, is advantageous, because primary production rates can be considered in different units, over different time scales and for different depths. This approach is particularly useful for sea ice science as very few data sets are available that present primary production rates. The time scales and investigated ice layers often vary between studies in ways that make direct comparison impossible.

The algorithm in our study does not account for diel changes in primary production-related parameters, such as E_k, and therefore does not represent the true net primary production (Harding et al., 1981). It is also important to keep in mind that the treatment of ice samples before and during the incubation experiment, to generate the PI curves, likely affects the algal community more than diel changes, as the melting of ice in darkness and the mixing, followed by sudden intense irradiation during the incubation, are far from natural conditions. The *in situ* incubation, on the other hand, only results in one value per depth, but describes the net primary production. Nevertheless, the samples for *in situ* incubation were also melted and mixed before being exposed to the natural light and temperatures at the same depth and, hence, measured primary production also differs from that under un-disturbed natural conditions.

The measured P^* for the 24-hour *in situ* incubations gave similar rates for all stations and vertical layers (P^* at St.1 surface: 0.02; P^* at St.1 bottom ice: 0.01; P^* at St.3 surface: 0.03; P^* at St.3 bottom ice: 0.01 μg C μg Chl a^{-1} h^{-1}) compared to the calculated results for St.3 (0.03 and 0.01 μg C μg Chl a^{-1} h^{-1} at the surface and bottom layers, respectively). The comparison with earlier studies is important for validating the methods applied in this study as the methodology in sea-ice studies, particularly for *in situ* measurements, is still challenging. We conclude that the methods applied in our study are valid, as the P^* values of the *in situ* and modelling approaches agree with results of other studies that investigated sea ice under similar conditions. *In situ* measurements in Antarctic sea ice showed P^* values of 0.02–0.056 μg C μg Chl a^{-1} h^{-1} in the bottom ice, but were higher in the ice interior with 0.7–1.17 μg C μg Chl a^{-1} h^{-1} (Mock, 2002). Calculated results for P^* at St.3 surface ice at maximum light levels were 0.12 μg C μg Chl a^{-1} h^{-1} and 0.09 μg C μg Chl a^{-1} h^{-1} at the top of the bottom ice. P^* was higher for the mean of both fast ice stations and GoF ice with 1.1 and 1.25 μg C μg Chl a^{-1} h^{-1} at the surface and 0.6 and 0.7 μg C μg Chl a^{-1} h^{-1} in the top of bottom ice, respectively. In Arctic and Antarctic sea ice, the measured rates are usually 0.03–2 μg C μg Chl a^{-1} h^{-1}, with maximum values of 5.2 and 8.6 μg C μg Chl a^{-1} h^{-1} (Gosselin et al., 1986; Cota and Smith, 1991; Lizotte and Sullivan, 1992; McMinn and Ashworth, 1998; summarised by Arrigo et al., 2010). The results of our study present the primary production rates for five vertical layers through the entire ice column. These *in situ* results along with the calculated primary production rates show that not only can light-absorbing parameters, such as CDOM or de-pigmented particles, be present at high concentrations in the upper layers, but other parameters linked to biological activity such as a_{algae} or Chl *a* can also be high. Upper layers therefore always need to be included in biological sea-ice studies and modelling, as also concluded by Gradinger (1999).

The calculated depth-integrated mean primary production per day (Figure 5a) was 166 μmol C m^{-2} d^{-1} for St.3 and higher for GoF with 1291 μmol C m^{-2} d^{-1} at mean PAR under ice of 9.3 μmol photons m^{-2} s^{-1} at St.3 and 15 μmol photons m^{-2} s^{-1} for GoF. Haecky and Andersson (1999) reported primary production rates for the Bothnian Bay in mid-March (200 μmol C m^{-2} d^{-1}) at similar light levels (6 μmol photons m^{-2} s^{-1}) as at St.3 in our study. The good agreement between the calculated primary production rates for St.3 and the measured ones by Haecky and Andersson (1999) supports the validity of our algorithm to calculate primary production. The calculated typical conditions in March in the Gulf of Finland ("GoF"-run) are characterised by higher light levels than measured by Haecky and Andersson (1999) in the northern Baltic Sea resulting in six times higher primary production rates in the Gulf of Finland.

The primary production rates in the Baltic Sea (St.3 surface, 4.8 mg C m^{-2} d^{-1}; St.3 bottom, 0.5 mg C m^{-2} d^{-1}; GoF surface, 34.1 mg C m^{-2} d^{-1}; GoF bottom, 5.6 mg C m^{-2} d^{-1}) are also in the same range as those reported in other regions: 0.2–463 mg C m^{-2} d^{-1} in the Arctic (Smith et al., 1988; Rysgaard et al., 2001) and 0.02–1249 mg C m^{-2} d^{-1} in Antarctic sea ice (Grossi et al., 1987), with the highest rates reported for Antarctic platelet ice. Annual primary production rates are up to 23 g C m^{-2} y^{-1} in the Arctic (Smith et al., 1988) and 38 g C m^{-2} y^{-1} in Antarctic sea ice (Grossi et al., 1987). An estimated 3–28% of the annual primary production of ice-covered polar waters takes place in sea ice (Legendre et al., 1992; Arrigo et al., 1998a, 1998b; Lizotte, 2001; Arrigo, 2003). In the Baltic Sea, Haecky and Andersson (1999) have estimated annual sea-ice primary production to be under 1% of the total annual primary production in the Baltic Sea. Moreover, they estimated that only 10% of the primary production during the ice-covered season took place in sea ice.

Methodological comparison

As a unique contribution, we present here the primary production calculations for each layer of the entire ice column over 24 hours based on optical parameters and compare them to primary production measurements. The high variability within our measured and calculated results shows not only the patchiness of ice and the variability due to the history of ice, but also the variability within and among earlier studies. Our study also indicates a method-dependent variability, as there are still a number of open questions regarding the treatment of samples and analysis methods. The *in situ* primary production estimates represent rather the net-primary production as they also include hours when only respiration could take place due to lack of light. The lab incubation, on the other hand, does not comprise any dark periods and the estimates are therefore closer to the gross primary production. The results of the lab incubation are thus higher compared to the *in situ* primary production rates. Another aspect that needs improvement in the future is the spectral range as the present version of the algorithm only covers the PAR regions. But since the effect of UV light on primary production is well known, the UV range should be included in future bio-optical models. Practical issues also likely affected the results of the *in situ* measurements and algorithm. The measurements from melted ice samples have temperatures higher than *in situ*. Elevated temperatures likely increase the primary production as increasing temperature is known to increase all activities in biological processes (Ralph et al., 2005). Applying the Q_{10} temperature coefficient, as defined by Arrigo et al. (1994) to be 1.9 for the growth of sea-ice algae, a temperature difference of 5 ˚C between the lab incubation and the *in situ* incubation would increase the algal growth rate by 38%. Our algorithm accounts for the estimated temperature difference between the incubator and the *in situ* conditions, but includes uncertainty as a temperature difference was not measured directly. Also, refreezing of the sample during the *in situ* incubation possibly has a negative effect on primary production as the sudden change in temperature causes stress for the organisms.

Another aspect that needs to be considered for the comparison between the calculated PP and the PP measured *in situ* is the available PAR. Although incubation was performed at a depth of 10 cm, the actual light field in the incubation hole must have differed from the natural situation for several reasons: the ice core that was placed on top of the sample vials was the original one from the hole, but was not adjusted to the ice surface due to logistical reasons. Hence, the core thickness was too high and the transmitted light lower than in undisturbed conditions. Additionally, brine drains out from the core during incubation, and will be replaced by gases. As gases have a higher scattering coefficient, their presence will also reduce the transmittance. The snow cover that was added on top of the incubation site was denser than the original one as it was compressed. This higher density may have two effects: further decreasing the transmittance and the albedo, which would then increase the transmittance. Another aspect that may increase the available light at the incubation site is the cut around the ice core that will allow light to penetrate directly down to the samples instead of through the ice. Air that was left within incubation vials to prevent breaking due to refreezing reduces the PAR available for the samples. Altogether these effects indicate that the available PAR for the *in situ* incubation was actually below that of undisturbed conditions at the same depth.

The sensitivity study showed that even small measurement inaccuracies, such as snow depth, light intensities or absorption properties, or incorrect parameterisation of the algorithm can cause large over- or underestimations in primary production that are hard to recognise due to the high natural variability and patchiness in primary production. One advantage of *in situ* incubations compared to lab incubations is the more realistic quality of light, as no artificial light source has been developed to mimic the complex changes in the quality of light during 24 hours in sea ice. A model, on the other hand, is only a simplification of the real conditions and cannot include all parameters controlling primary production. In the case of our study, absorption properties and primary production-specific parameters were averaged for the entire surface and the entire bottom layer, respectively. The algorithm may therefore have been less accurate than *in situ* measurements based on multi-layer samples. These multi-layer samples, on the other hand, were incubated together at one depth and therefore exposed the photosynthetic organisms adapted to bottom layers to higher light levels and the surface communities to lower light levels than under natural conditions. The focus should therefore be on the second layer (11–22 cm) when comparing the two methods. The mean of the calculated primary production in surface ice and bottom ice, respectively, agrees relatively well with the mean of the *in situ* measurements at both layers.

Additionally to the limitations in the methods, the comparison of *in situ* and calculated results for St.3 again show an over-estimation of primary production rates by the algorithm. This over-estimation implies either inaccuracies in the measured input parameters for the algorithm or that the algorithm is missing a parameter that has not been identified with the current state of our knowledge.

We conclude that the true primary production likely lies between the measured and the calculated results and, hence, either method can be applied, accounting for associated limitiations, to arrive at a reasonable estimate of primary production in Baltic Sea ice under similar conditions. For *in situ* measurements of primary production, the method applied here can be improved, for example, by incubating all samples at their original depth of origin. Only measuring primary production in sea ice under undisturbed conditions, however, can provide accurate results. For very cold conditions and more saline ice, the algorithm will need to be adjusted.

Nutrients have been found to be the main limiting factor for primary production in Arctic sea ice (Gradinger et al., 2009). As they were not limited in our present study (Table S1), and were sometimes even highest in the top layers, possibly due to the flooding or atmospheric depositions (Granskog et al., 2003), nutrient concentrations were not considered in the algorithm.

Conclusions

This study presents a unique combination of optical, biogeochemical and biological measurements for different types of Baltic Sea ice. The results agree with earlier studies on the different optical or biological properties of Baltic Sea ice. The station in our study that combined all measurements (St.3) was characterised by high snow, slush and ice depth and therefore comparably low light levels in the ice. Hence, the primary production rates resulting from our algorithm are in the low range of published measurements. The calculated typical rates of primary production for the Gulf of Finland are higher, with 15.6 mg C m^{-2} d^{-1} at mean daily PAR levels.

The importance of optical and biogeochemical processes in ice on the regional and global carbon cycle and the heat budget can only be shown by large datasets and ecosystem models. The approach of combining optical, biogeochemical and biological measurements with modelling in our present study supports the development of complex ecosystem models by providing input data for modelling. The comparison among different ice types in the Gulf of Finland and with *in situ* measurements helps to develop reliable sampling methods and to understand the variability and functioning of the sea-ice ecosystem.

The results of our study can support future models as the sensitivity study showed that E_k values (based on PI relationships) have only little effect on the primary production rates compared to snow depth or absorption properties. The maximum quantum yield ϕ_{max} in our present study also significantly affected the calculated primary production rates. Variation among the mean ϕ_{max} of surface ice and bottom ice at all stations was not significant, suggesting that one value for modelling the entire ice layer may be sufficient.

Appendix

Abbreviations

Abbreviation	Units	Definitions
E_d	mol photons m^{-2} d^{-1}	Measured plane downwelling incident irradiance
E_0	µmol photons m^{-2} s^{-1}	Calculated scalar downwelling irradiance
E_k	µmol photons m^{-2} s^{-1}	Light saturation index
PAR	mol photons m^{-2} d^{-1}	Photosynthetically active radiation, summed over the active region of irradiance (400–700 nm)
b	m^{-1}	Light scattering coefficient
$a_{CDOM}(\lambda)$	m^{-1}	Absorption coefficient of chromophoric dissolved organic matter
$a_t(\lambda)$	m^{-1}	Total absorption coefficient including non-algal particles and phytoplankton-related particles
$a_d(\lambda)$	m^{-1}	Absorption coefficient of de-pigmented particles
$a_{algae}(\lambda)$	m^{-1}	Absorption coefficient of phytoplankton-related particles
$a_{algae}^*(\lambda)$	m^2 mg Chl a^{-1}	Chl *a*-specific absorption coefficient of phytoplankton-related particles
$\bar{a}^*$	m^2 mg Chl a^{-1}	Wavelength-dependent, Chl *a*-specific absorption by all pigments
ϕ	mol C mol photons^{-1}	Quantum yield for C fixation based on photosynthesis
ϕ^*_{max}	mol C mol photons^{-1}	Maximum quantum yield for C fixation based on photosynthesis
α	mg C mg Chl a^{-1} h^{-1} [µmol photons m^{-2} s^{-1}]$^{-1}$	Maximum light utilisation coefficient
β	g C m^2 g Chl a^{-1} mol photons^{-1}	photoinhibition parameter
P_m	µg C m^{-3} h^{-1}, µg C µg Chl a^{-1} h^{-1}	Maximum photosynthetic rate, which can also be normalized to Chl *a* concentration
P	µg C m^{-3} h^{-1}, or mg C m^{-2} d^{-1}	Primary production rate per volume, or per column of ice
P^*	µg C µg Chl a^{-1} h^{-1}	Primary production rate normalized to Chl *a* concentration
Chl *a*	µg Chl *a* L^{-1}	Chlorophyll *a* concentration, measured by fluorometer

References

Arrigo KR. 1997. Primary production in Antarctic sea ice. *Science* **276**: 394–397.

Arrigo KR. 2003. Primary production in sea ice, in Thomas DN, Dieckmann GS, eds., *Sea Ice - An Introduction to Its Physics, Biology, Chemistry and Geology*. London: Blackwell Science. pp. 143–183.

Arrigo KR, Mock T, Lizotte MP. 2010. Primary producers and sea ice, in Thomas DN, Dieckmann GS, eds., *Sea Ice*. 2nd ed. Oxford: Wiley-Blackwell Publishing. pp. 283–325.

Arrigo KR, Sullivan CW. 1994. A high resolution bio-optical model of microalgal growth: Tests using sea-ice algal community time-series data. *Limnol Oceanogr* **39**(3): 609–631.

Arrigo KR, Sullivan CW, Kremer JN. 1991. A bio-optical model of Antarctic sea ice. *J Geophys Res* **96**(C6): 10581. doi:10.1029/91JC00455.

Arrigo KR, Worthen D, Schnell A, Lizotte MP. 1998b. Primary production in Southern Ocean waters. *J Geophys Res* **103**(C8): 15587–15600.

Arrigo KR, Worthen DL, Dixon P, Lizotte MP. 1998a. Primary productivity of near surface communities within Antarctic pack ice. *Antarctic Research Series* **73**: 23–43.

Babin M, Stramski D, Ferrari GM, Claustre H, Bricaud A, et al. 2003. Variations in the light absorption coefficients of phytoplankton, nonalgal particles, and dissolved organic matter in coastal waters around Europe. *J Geophys Res* **108**(C7).

Behrenfeld MJ, Falkowski PG. 1997. Photosynthetic rates derived from satellite-based chlorophyll concentration. *Limnol Oceanogr* **42**(1): 1–20.

Bidigare RR, Prezelin BB, Smith RC, Barbara S. 1992. Bio-optical models and the problems of scaling, in Falkowski PG, Woodhead AD, eds., *Primary Production and Biogeochemical Cycles in the Sea*. New York: Plenum Press. pp. 175–212.

Cota GF, Smith REH. 1991. Ecology of bottom ice algae: II. Dynamics, distributions and productivity. *J Marine Syst* **2**: 279–295.

Ehn J, Granskog MA, Reinart A, Erm A. 2004. Optical properties of melting landfast sea ice and underlying seawater in Santala Bay, Gulf of Finland. *J Geophys Res* **109**: 1–12.

Ehn JK, Mundy CJ. 2013. Assessment of light absorption within highly scattering bottom sea ice from under-ice light measurements: Implications for Arctic ice algae primary production. *Limnol Oceanogr* **58**(3): 893–902.

Ehn JK, Mundy CJ, Barber DG. 2008b. Bio-optical and structural properties inferred from irradiance measurements within the bottommost layers in an Arctic landfast sea ice cover. *J Geophys Res* **113**(C3): C03S03.

Ehn JK, Papakyriakou TN, Barber DG. 2008a. Inference of optical properties from radiation profiles within melting landfast sea ice. *J Geophys Res* **113**(C9): C09024.

Enberg S, Piiparinen J, Majaneva M, Vähätalo AV, Autio R, et al. 2015. Solar PAR and UVR modify the community composition and photosynthetic activity of sea ice algae. *FEMS Microbiol Ecol* **91**. doi: 10.1093/femsec/fiv102 fiv102.

Eppley RW. 1972. Temperature and phytoplankton growth in the sea. *Fish Bull* **70**(4).

Falkowski PG, Raven JA. 2007. Photosynthesis and primary production in nature, in Falkowski PG, Raven JA, eds., *Aquatic Photosynthesis*. Princeton: Princeton University Press. pp. 319–363.

Ferrari GM, Tassan S. 1999. A method using chemical oxidation to remove light absorption by phytoplankton pigment. *J Phycol* **35**: 1090–1098.

Gibson JAE, Vincent WF, Nieke B, Pienitz R. 2000. Control of biological exposure to UV radiation in the Arctic Ocean: Comparison of the roles of ozone and riverine dissolved organic matter. *Arctic* **53**(4): 372–382.

Glud RN, Rysgaard S, Kühl M. 2002. A laboratory study on O_2 dynamics and photosynthesis in ice algal communities: Quantification by microsensors, O_2 exchange rates, C incubations and a PAM fluorometer. *Aquat Microb Ecol* **27**: 301–311.

Gosselin M, Legendre L, Therriault J, Demers S, Rochet M. 1986. Physical control of the horizontal patchiness of sea-ice microalgae. *Mar Ecol-Prog Ser* **29**: 289–298.

Gradinger R. 1999. Vertical fine structure of the biomass and composition of algal communities in Arctic pack ice. *Mar Biol* **133**(August 1991): 745–754.

Gradinger R. 2009. Sea-ice algae: Major contributors to primary production and algal biomass in the Chukchi and Beaufort Seas during May/June 2002. *Deep-Sea Res Pt II* **56**(17): 1201–1212.

Granskog MA. 2004. Seasonal development of the properties and composition of landfast sea ice in the Gulf of Finland, the Baltic Sea. *J Geophys Res* **109**(C2): 1–11.

Granskog MA, Kaartokallio H, Shirasawa K. 2003. Nutrient status of Baltic Sea ice: Evidence for control by snow-ice formation, ice permeability, and ice algae. *J Geophys Res* **108**(C8): 3253. doi: 10.1029/2002JC001386.

Grenfell TC, Perovich DK. 1981. Radiation absorption coefficients of polycrystalline ice from 400–1400 nm. *J Geophys Res* **86**(C8): 7447–7450.

Grossi M, Kottmeier S, Moe R, Taylor G, Sullivan C. 1987. Sea ice microbial communities. VI. Growth and primary production in bottom ice under graded snow cover. *Mar Ecol-Prog Ser* **35**: 153–164.

Haecky P, Andersson A. 1999. Primary and bacterial production in sea ice in the northern Baltic Sea. *Aquat Microb Ecol* **20**: 107–118.

Hänninen S, Nyman T, Rytkönen J, Rosqvist T, Sonninen S, et al. 2002. The implementation of the VTMIS system for the Gulf of Finland. *Research Report NO VAL34–013153*. VTT Technical Research Centre of Finland.

Harding LA, Prezelin BB, Sweeney BM, Cox JL. 1981. Diel oscillations in the photosynthesis-irradiance relationship of a planktonic marine diatom. *J Phycol* **17**: 389–394.

Helms JR, Stubbins A, Ritchie JD, Minor EC, Kieber DJ, et al. 2008. Absorption spectral slopes and slope ratios as indicators of molecular weight, source, and photobleaching of chromophoric dissolved organic matter. *Limnol Oceanogr* **53**(3): 955–969.

Hyvärinen AP, Kolmonen P, Kerminen VM, Virkkula A, Leskinen A, et al. 2011. Aerosol black carbon at five background measurement sites over Finland, a gateway to the Arctic. *Atmos Environ* **45**: 4042–4050.

Jalkanen L, Mäkinen A, Häsänen E, Juhanoja J. 2000. The effect of large anthropogenic particulate emissions on atmospheric aerosols, deposition and bioindicators in the eastern Gulf of Finland region. *Sci Total Environ* **262**: 123–136.

Järvinen O, Leppäranta M. 2011. Transmission of solar radiation through the snow cover on floating ice. *J Glaciol* **57**(205): 861–870.
Jassby AD, Platt T. 1976. Mathematical formulation of the relationship photosynthesis and light for phytoplankton. *Limnol Oceanogr* **21**(4): 540–547.
Kaartokallio H, Kuosa H, Thomas DN, Granskog MA, Kivi K. 2007. Biomass, composition and activity of organism assemblages along a salinity gradient in sea ice subjected to river discharge in the Baltic Sea. *Polar Biol* **30**: 183–197.
Kiefer DA, Mitchell B. 1983. A simple, steady-state description of phytoplankton growth based on absorption cross-section and quantum efficiency. *Limnology* **28**: 770–776.
Kirk JTO. 1994. *Light and photosynthesis in aquatic ecosystems*. Cambridge: Cambridge University Press.
Kishino M, Takahashi M, Okami N, Ichimura S. 1985. Estimation of the spectral absorption-coefficients of phytoplankton in the sea. *B Mar Sci* **37**(2): 634–642.
Kuivikko M, Kotiaho T, Hartonen K, Tanskanen A, Vähätalo AV. 2007. Modeled direct photolytic decomposition of polybrominated diphenyl ethers in the Baltic Sea and the Atlantic Ocean. *Environ Sci Technol* **41**(20): 7016–7021.
Legendre L, Ackley SF, Dieckmann GS, Gulliksen B, Horner R, et al. 1992. Ecology of sea ice biota. *Polar Biol* **12**(3–4): 429–444.
Lizotte MP. 2001. The contributions of sea ice algae to antarctic marine primary production. *Am Zool* **41**: 57–73.
Lizotte MP, Priscu C. 1994. Natural fluorescence and quantum yields in vertically stationary phytoplankton from perennially ice-covered lakes. *Limnol Oceanogr* **39**(6): 1399–1410.
Lizotte MP, Sullivan CW. 1992. Photosynthetic capacity in microalgae associated with Antarctic pack ice. *Polar Biol* **12**(5): 497–502.
Long MH, Koopmans D, Berg P, Rysgaard S, Glud RN, et al. 2012. Oxygen exchange and ice melt measured at the ice-water interface by eddy correlation. *Biogeosciences* **9**: 1957–1967.
Matsuoka A, Larouche P, Poulin M, Vincent W, Hattori H. 2009. Phytoplankton community adaptation to changing light levels in the southern Beaufort Sea, Canadian Arctic. *Estuar Coastal Shelf S* **82**(3): 537–546.
McMinn A, Ashworth C. 1998. The use of oxygen microelectrodes to determine the net production by an Antarctic sea ice algal community. *Antarctic Sci* **10**(1): 39–44.
Melbourne-Thomas J, Meiners K, Mundy C, Schallenberg C, Tattersall K, et al. 2015. Algorithms to estimate Antarctic sea ice algal biomass from under-ice irradiance spectra at regional scales. *Mar Ecol-Prog Ser* **536**: 107–121.
Mock T. 2002. In situ primary production in young Antarctic sea ice. *Hydrobiologia* **470**: 127–132.
Mock T, Gradinger R. 1999. Determination of Arctic ice algal production with a new in situ incubation technique. *Mar Ecol-Prog Ser* **177**: 15–26.
Mock T, Kruse M, Dieckmann GS. 2003. A new microcosm to investigate oxygen dynamics at the sea ice water interface. *Aquat Microb Ecol* **30**: 197–205.
Morel A. 1988. Optical modeling of the upper ocean in relation to its biogenous matter content (case I waters). *J Geophys Res* **93**(C9): 10,749–10,768.
Morel A. 1991. Light and marine photosynthesis: A spectral model with geochemical and climatological implications. *Prog Oceanogr* **26**(3): 263–306.
Müller S, Vähätalo AV, Granskog MA, Autio R, Kaartokallio H. 2011. Behaviour of dissolved organic matter during formation of natural and artificially grown Baltic Sea ice. *Ann Glaciol* **52**(57): 233–241.
Mundy CJ, Gosselin M, Ehn JK, Belzile C, Poulin M, et al. 2011. Characteristics of two distinct high-light acclimated algal communities during advanced stages of sea ice melt. *Polar Biol* **34**(12): 1869–1886.
Nicolaus M, Gerland S, Hudson SR, Hanson S, Haapala J, et al. 2010b. Seasonality of spectral albedo and transmittance as observed in the Arctic Transpolar Drift in 2007. *J Geophys Res* **115**(C11): C11011.
Nicolaus M, Hudson SR, Gerland S, Munderloh K. 2010a. A modern concept for autonomous and continuous measurements of spectral albedo and transmittance of sea ice. *Cold Reg Sci Technol* **62**(1): 14–28.
Nicolaus M, Katlein C. 2013. Mapping radiation transfer through sea ice using a remotely operated vehicle (ROV). *The Cryosphere* **7**(3): 763–777.
Perovich DK. 1990. Theoretical Estimates of Light Reflection and Transmission by Spatially Complex and Temporally Varying Sea Ice Covers. *J Geophys Res* **95**(C6): 9557–9567.
Perovich DK. 2003. Complex yet translucent: The optical properties of sea ice. *Physica B* **338**: 107–114.
Perovich DK, Govoni JW. 1991. Absorption coefficients of ice from 250 to 400 nm. *Geophys Res Lett* **18**(7): 1233–1235.
Piiparinen J. 2011. Fast- and drift-ice communities in the Bothnian Bay and the impact of UVA ratiation on the Baltic Sea ice ecology. *W & A de Nottbeck Foundation Sci Rep* **36**.
Piiparinen J, Enberg S, Rintala J-M, Sommaruga R, Majaneva M, et al. 2015. The contribution of mycosporine-like amino acids, chromophoric dissolved organic matter and particles to the UV protection of sea-ice organisms in the Baltic Sea. *Photochem Photobiol* **14**: 1025–1038.
Piiparinen J, Kuosa H, Rintala J-M. 2010. Winter-time ecology in the Bothnian Bay, Baltic Sea: Nutrients and algae in fast ice. *Polar Biol* **33**(11): 1445–1461.
Pirazzini R, Vihma T, Granskog MA, Cheng B. 2006. Surface albedo measurements over sea ice in the Baltic Sea during the spring snowmelt period. *Ann Glaciol* **44**(1): 7–14.
Platt T, Gallegos CL, Harrison WG. 1980. Photoinhibition of photosynthesis in natural assemblages of marine phytoplankton. *J Mar Res* **38**:103–111.
Raateoja M, Seppälä J, Kuosa H. 2004. Bio-optical modelling of primary production in the SW Finnish coastal zone, Baltic Sea: Fast repetition rate fluorometry in Case 2 waters. *Mar Ecol-Prog Ser* **267**: 9–26.
Ralph PJ, McMinn A, Ryan KG, Ashworth C. 2005. Short-term effect of temperature on the photokinetics of microalgae from the surface layers of Antarctic pack ice. *J Phycol* **41**(4): 763–769.
Rintala J-M, Piiparinen J, Blomster J, Majaneva M, Müller S, et al. 2014. Fast direct melting of brackish sea-ice samples results in biologically more accurate results than slow buffered melting. *Polar Biol* **37**: 1811–1822.

Rintala J-M, Piiparinen J, Uusikivi J. 2010. Drift-ice and under-ice water communities in the Gulf of Bothnia (Baltic Sea). *Polar Biol* **33**(2): 179–191.
Rysgaard S, Kühl M, Glud RN, Würgler Hansen J. 2001. Biomass, production and horizontal patchiness of sea ice algae in a high-Arctic fjord (Young Sound, NE Greenland). *Mar Ecol-Prog Ser* **223**: 15–26.
Sakshaug E, Johnsen G, Andresen K, Vernet M. 1991. Modeling of light-dependent algal photosynthesis and growth: Experiments with the Barents Sea diatoms ***Thalassiosira nordenskioeldii*** and ***Chaetoceros furcellatus***. *Deep-Sea Res* **38**(4): 415–430.
Setälä O. 2004. Studies on planktonic brackish water microprotozoans with special emphasis on the role of ciliates as grazers. *W & A de Nottbeck Foundation Sci Rep* **25**.
Smith RC, Baker KS. 1981. Optical properties of the clearest natural waters (200–800 nm). *Appl Optics* **20**(2): 177–84.
Smith REH, Anning J, Cota G. 1988. Abundance and production of ice algae in Resolute Passage, Canadian Arctic. *Mar Ecol-Prog Ser* **48**: 251–263.
Smith ARC, Prezelin BB, Bidigare RR, Baker KS. 1989. Bio-optical modelling of photosynthetic production in coastal waters. *Limnol Oceanogr* **34**(8): 1524–1544.
Sogandares FM, Fry ES. 1997. Absorption spectrum (340–640 nm) of pure water. I. Photothermal measurements. *Appl Optics* **36**(33): 8699–8709.
Stedmon C, Markager S, Kaas H. 2000. Optical Properties and Signatures of Chromophoric Dissolved Organic Matter (CDOM) in Danish Coastal Waters. *Estuar Coastal Shelf S* **51**: 267–278.
Stedmon CA, Thomas DN, Granskog M, Kaartokallio H, Papadimitriou S, et al. 2007. Characteristics of dissolved organic matter in Baltic coastal sea ice: Allochthonous or autochthonous origins? *Environ Sci Technol* **41**(21): 7273–7279.
Steemann-Nielsen E. 1952. The use of radioactive carbon (^{14}C) for measuring organic production in the sea. *J Cons Int Explor Mer* **18**: 117–140.
Stoecker DK, Gustafson DE, Baier CT, Black MMD. 2000. Primary production in the upper sea ice. *Aquat Microb Ecol* **21**: 275–287.
Subramaniam A, Carpenter EJ, Falkowski PG. 1999. Bio-optical properties of the marine diazotrophic cyanobacteria ***Trichodesmium*** spp. II. A reflectance model for remote-sensing. *Limnol Oceanogr* **44**(3): 618–627.
Tassan S, Ferrari GM. 2002. A sensitivity analysis of the "Transmittance – Reflectance" method for measuring light absorption by aquatic particles. *J Plankton Res* **24**: 757–774.
Tedesco L, Vichi M, Haapala J, Stipa T. 2010. A dynamic biologically active layer for numerical studies of the sea ice ecosystem. *Ocean Modelling* **35**(1–2): 89–104.
Tedesco L, Vichi M, Thomas DN. 2012. Process studies on the ecological coupling between sea ice algae and phytoplankton. *Ecol Model* **226**: 120–138.
Uusikivi J, Vähätalo AV, Granskog MA, Sommaruga R. 2010. Contribution of mycosporine-like amino acids and colored dissolved and particulate matter to sea ice optical properties and ultraviolet attenuation. *Limnol Oceanogr* **55**(2): 703–713.
Vancoppenolle M, Bopp L, Madec G, Dunne J, Ilyina T, et al. 2013. Future arctic ocean primary productivity from CMIP5 simulations: Uncertain outcome, but consistent mechanisms. *Global Biogeochem Cy* **27**: 605–619.
Weeks WF, Gow AJ. 1978. Preferred crystal orientations in the fast ice along the margins of the Arctic Ocean. *J Geophys Res* **83**: 5105–5121.
Zhao J-P, Li T, Barber D, Ren J-P, Pucko M, et al. 2010. Attenuation of lateral propagating light in sea ice measured with an artificial lamp in winter Arctic. *Cold Reg Sci Technol* **61**(1): 6–12.

Contributions

- Contributed to conception and design: SuM, AVV, RA, JMR, JU
- Contributed to acquisition of data: SuM, JU, MM, SaM, JMR
- Contributed to analysis and interpretation of data: SuM, AVV, JU, MM, SaM, RA, JMR
- Drafted and revised the article: SuM, AVV, JU, MM, SaM, RA, JMR
- Approved and submitted version for publication: SuM

Acknowledgments

We gratefully acknowledge the support of crew members and other researchers onboard of the R/V *Aranda* and thank the cruise leader Jari Haapala for including the ice biologists and for fruitful collaboration during the cruise. Ilkka Lastumäki is acknowledged for the nutrient analysis and the support with scientific diving together with Tuomo Roine. We thank Ilkka Matero for ice structure analysis. The laboratory analysis was done at the facilities of Tvärminne Zoological station and we thank the skilled staff and the Walter and Andrée de Nottbeck Foundation for the support.

Funding information

This work has been funded by the Walter and Andrée de Nottbeck foundation by financing the field work and providing personal grants to SuM, JMR, MM, JU and SaM. Furthermore, the Finnish Environment Insistitut (SYKE) funded the work of RA and JU. SaM also received funding through the Onni Talas Foundation.

Competing interests

The authors have no competing interests, as defined by Elementa, that might be perceived to influence the research presented in this manuscript.

Supplemental material

- **Figure S1. Absorption spectra of CDOM at all stations.**
  Absorption spectra of CDOM for sea ice at St.1 (drift ice), St.2 (deformed fast ice), St.3 (level fast ice) and St.4 (level fast ice). The results for all ice layers that were analysed in each station are shown. The absorption of CDOM in under-ice water (UIW) and slush in all stations are shown in the lowest panel.
  doi: 10.12952/journal.elementa.000121.s001

- **Figure S2. Absorption spectra of algae at all stations.**
  Absorption spectra of algae for sea ice at St.1 (drift ice), St.2 (deformed fast ice), St.3 (level fast ice) and St.4 (level fast ice). The results for all ice layers that were analysed in each station are shown. The absorption of algae in under-ice water (UIW) and slush in all stations are shown in the lowest panel.
  doi: 10.12952/journal.elementa.000121.s002
- **Figure S3. Absorption spectra of de-pigmented particles at all stations.**
  Absorption spectra of de-pigmented particles for sea ice at St.1 (drift ice), St.2 (deformed fast ice), St.3 (level fast ice) and St.4 (level fast ice). The results for all ice layers that were analysed in each station are shown. The absorption of de-pigmented particles in under-ice water (UIW) and slush in all stations are shown in the lowest panel.
  doi: 10.12952/journal.elementa.000121.s003

Data accessibility statement

Data available from the Dryad Digital Repository: http://dx.doi.org/10.5061/dryad.7k1gf.